ELSEVIER

Journal of Contaminant Hydrology 31 (1998) 373–407

JOURNAL OF
Contaminant
Hydrology

Nonlinear sorption and nonequilibrium solute transport in aggregated porous media: Experiments, process identification and modeling

Claudia Fesch [a], Werner Simon [b,1], Stefan B. Haderlein [a,*], Peter Reichert [b,*], René P. Schwarzenbach [a]

[a] *Department of Chemistry, Swiss Federal Institute for Environmental Science and Technology (EAWAG) and Swiss Federal Institute of Technology (ETH), 8600 Dübendorf, Switzerland*

[b] *Department of Computer and System Sciences, Swiss Federal Institute for Environmental Science and Technology (EAWAG) and Swiss Federal Institute of Technology (ETH), 8600 Dübendorf, Switzerland*

Received 11 March 1997; revised 24 September 1997; accepted 24 September 1997

Abstract

The combined effects of nonlinear sorption, nonequilibrium mass transfer and the distribution of sorption sites on transport of organic contaminants has been examined in porous media containing aggregates of clay minerals and organic matter as sorbents. The major goal was to develop general concepts for describing, deterministically, the transport processes of solutes with different adsorption characteristics in such systems. Various sets of batch adsorption and miscible displacement experiments were performed covering a wide range of time scales and other experimental conditions. Using a multiple reactive tracer approach, independent information was obtained on the hydrodynamic properties of the columns, on the relative importance of the two different sorbents present, and on the accessibility and the distribution of these sorbents at the pore scale. The breakthrough curves (BTCs) of the nonlinearly sorbing tracer generally exhibited sharp fronts and excessive tailing, consistent with the Langmuir–Freundlich type adsorption at clays. The effect of nonequilibrium mass transfer was most evident from the tailing of the self-sharpened fronts of the BTCs and from the results of interrupted flow experiments. A two-region model, which incorporated nonlinear sorption and retarded intra-aggregate diffusion, successfully described the results of our entire set of miscible displacement data using a *single* set of parameter values. Our study demonstrates that although nonlinear sorption and nonequilibrium mass transfer may have very similar effects on solute BTCs, these processes can be distinguished from

* Corresponding authors. Fax: +41-1-823-5028; e-mail: haderlein@eawag.ch\reichert@eawag.ch.

[1] Present address: Institute of Industrial Mathematics, Erwin-Schrödinger-Str. 49, 67633 Kaiserslautern, Germany.

PII S0169-7722(97)00078-8

experimental data if experiments with different solutes, different flow rates and different input concentrations are evaluated simultaneously. It is shown that a very small volume fraction of immobile regions ($< 0.1\%$ of total porosity), which is insignificant for the transport of conservative solutes, may strongly affect the transport of sorbing solutes if sorption sites are concentrated within these regions. In soils and aquifers, clay minerals and other reactive surfaces are often present in aggregates. Thus, the transport of solutes that strongly interact with such sites generally is very susceptible to rate-limited mass transfer processes while the transport of conservative tracers is poorly affected. © 1998 Elsevier Science B.V.

Keywords: Solute transport; Nonlinear sorption; Two-region model; Retarded intra-particle diffusion; Porous media; Breakthrough curves

1. Introduction

Sorption to the solid matrix of soils and aquifers is one of the key processes that determine the fate of contaminants in the subsurface. Not only transport but also bioavailability and transformation of toxic chemicals may be strongly affected by interactions with solid surfaces (Schweich and Sardin, 1981; Ogram et al., 1985; Miller and Alexander, 1991; Weber et al., 1991; McBride et al., 1992; Harms and Zehnder, 1995). Examples of such processes include ion exchange (Talibudeen, 1981; Sposito, 1990), specific adsorption of trace metals (Sigg, 1987) or organic pollutants (Haderlein and Schwarzenbach, 1993; Stone et al., 1993), or heterogeneous hydrolysis (Torrents and Stone, 1991) or redox reactions (Voudrias and Reinhard, 1986; Klausen et al., 1995). In natural porous media, however, reactive surface sites such as clay minerals, or iron- and manganese oxides may be poorly accessible due to their presence in immobile regions where advective water flow is insignificant. Fig. 1 schematically illustrates such conditions in a porous medium with immobile regions. In contrast to nonreactive solutes, diffusion-limited mass transfer even into a very small fraction of such immobile regions may significantly affect the transport or the transformation of *reactive* chemicals if a significant fraction of reactive sites is located therein (Young and Ball, 1994).

Mass transfer of sorbing solutes may be affected by both, chemical and physical nonequilibrium processes (see reviews of Sardin and Schweich, 1991; Jury and Flühler, 1992; Brusseau, 1994; Pignatello and Xing, 1996). On the one hand, chemical reactions between solutes and sorbents may be slow compared to the respective physical transport processes. This *chemical nonequilibrium* results in early breakthrough and/or tailing of solute breakthrough curves (BTCs) in miscible displacement experiments. On the other hand, nonequilibrium may be due to solute diffusion into stagnant or immobile regions of the porous medium. Such *physical nonequilibrium* also gives rise to early breakthrough and/or tailing of BTCs, but affects both conservative and sorbing solutes. Various models have been developed to describe nonequilibrium solute transport in porous media. The most common approaches include two-site models, which refer to chemical nonequilibrium, or two-region models, which account for physical nonequilibrium (Coats and Smith, 1964; Selim et al., 1976; van Genuchten and Wierenga, 1976a; Cameron and Klute, 1977). Recently, models were introduced that account for more than one mass transfer process (Haggerty and Gorelick, 1995; Xu and Brusseau, 1996; Yiacoumi and Rao, 1996).

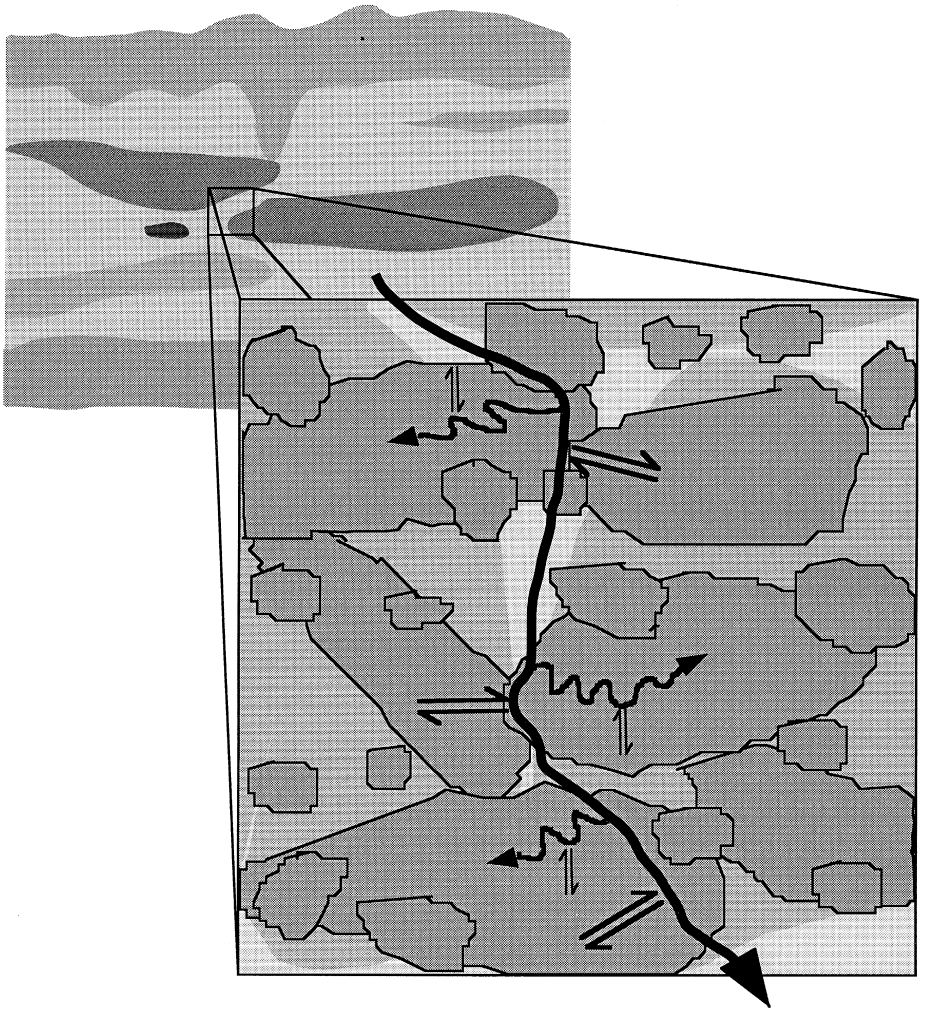

Fig. 1. Schematic illustration of a section of a porous medium that contains reactive fine particles (dark). Aggregation of those particles creates immobile regions where mass transfer occurs by diffusion only. Arrows indicate advective (thick line) and diffusive (thin lines) solute flux, respectively. Sorption (double arrows) may take place in both regions.

In most cases, such transport models were applied to solutes, for which linear sorption isotherms could be assumed. However, interactions of pollutants with mineral surfaces often give rise to strongly nonlinear adsorption isotherms (Zachara et al., 1990; Haderlein et al., 1996). The effects of sorption nonlinearity and nonequilibrium mass transfer on solute transport have been evaluated primarily in the field of nonlinear chromatography (Helfferich and Carr, 1993). Several studies related these ideas to solute transport in subsurface environments. A numerical simulation model presented by van Genuchten and Wierenga (1976b) combined advective–dispersive transport with nonlin-

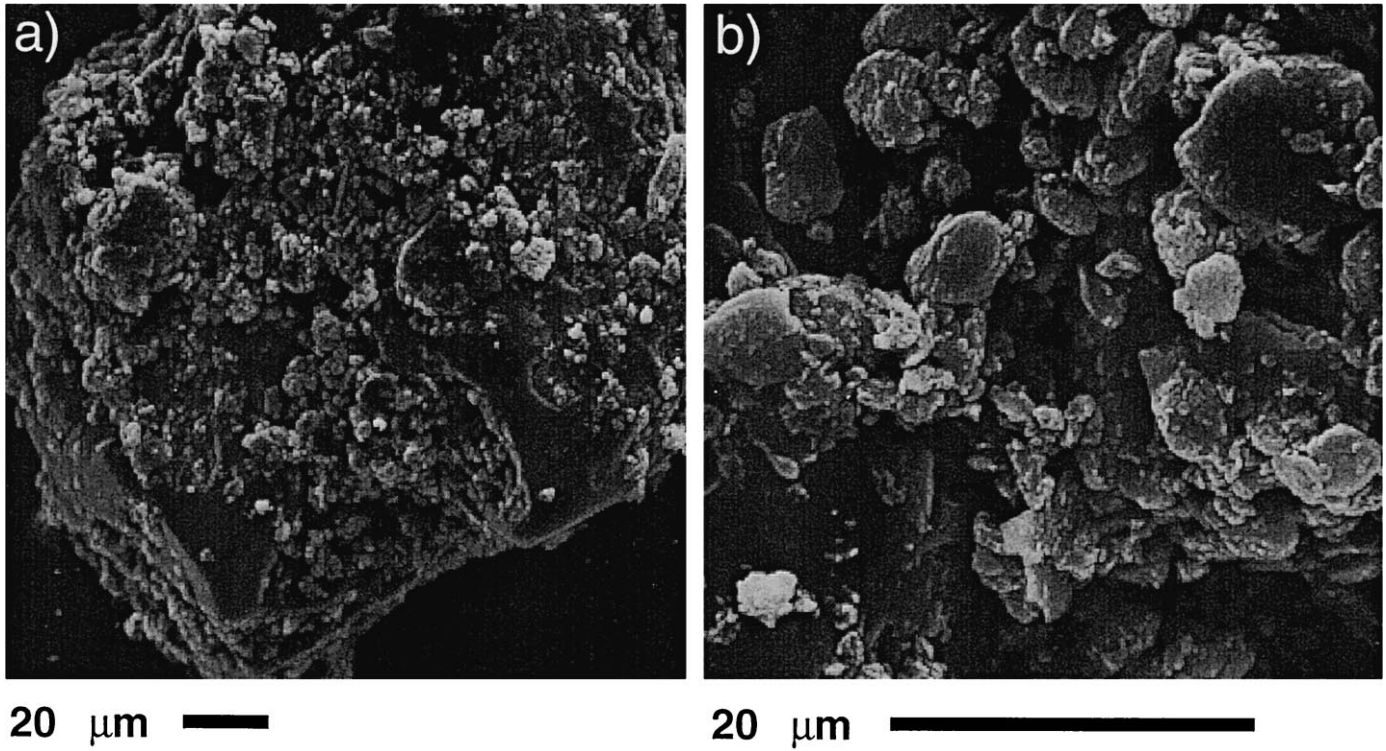

Fig. 2. REM (raster electron microscope) enlargements of the clay coated sand particles used in this study. (a) Various arrangements of clay aggregates on a single grain of quartz sand. (b) Microporosity of aggregated clay minerals. The basal surfaces of single montmorillonite crystals are visible.

ear sorption and intra-aggregate diffusion, but was restricted to cases with weak sorption nonlinearity and relatively strong dispersive effects. Simulations of Bosma and van der Zee (1995) and Berglund and Cvetkovic (1996) showed that also in heterogeneous porous media, the shape of solute sorption isotherms may have a strong impact on the shape of solute BTCs. The importance of both, nonlinear sorption and nonequilibrium processes was also shown in experimental studies (van der Zee and van Riemsdijk, 1986; Spurlock et al., 1995).

To date, there is, however, still a lack of process oriented *experimental* studies that allow a better *identification* and *quantification* of the combined effects of nonlinear chemical processes at surfaces and nonequilibrium mass transfer on solute transport in aggregated porous media. An extended data base is needed to obtain a better understanding of the interplay and relative importance of such coupled processes in structured porous media.

In this work, the transport of nonlinearly sorbing solutes was studied in a structured porous medium under saturated flow conditions in laboratory columns. To evaluate the effects of nonlinearly retarded mass transfer within immobile regions, a solid matrix was developed that exhibits immobile regions that host a significant fraction of the sorption sites. These regions consist of aggregated clay minerals that are attached to inert quartz sand (see Fig. 2). 1,3-Dinitrobenzene (DNB) was chosen as reactive tracer since it strongly sorbs to clay minerals exhibiting distinctly nonlinear sorption isotherms (Haderlein et al., 1996; Weissmahr et al., 1998). In addition to this specific sorption to clay minerals, DNB is subject to hydrophobic partitioning into organic matter, which is also present in our system. To quantify these two sorption processes as well as the hydrodynamic transport processes, additional tracers were chosen: two alkyl phenols exhibiting linear sorption isotherms were used as hydrophobic partitioning tracers and thiourea was used as a conservative tracer.

Batch equilibrium adsorption isotherms of the solutes were compared to in situ sorption isotherms calculated from solute BTCs. The column experiments covered a wide range of flow velocities and solute concentrations. Interrupted flow experiments were carried out to further investigate nonequilibrium processes within the columns.

The data of the miscible displacement experiments were modeled using a novel version of the data analysis program AQUASIM (Simon and Reichert, 1997). Models of various degrees of complexity were tested for process identification and parameter estimation in order to consistently describe the transport of the different tracers in the aggregated model system. In particular, the effects of nonlinear sorption, nonequilibrium mass transfer with and within immobile regions, and the distribution of reactive sites within such regions on solute transport were evaluated.

2. Materials and methods

2.1. Sorbents

Three types of sorbents were used: (1) pure quartz sand, (2) quartz sand coated with polyvinyl alcohol (PVA) (referred to as sandPVA) and (3) quartz sand coated with a mixture of the clay mineral montmorillonite and PVA (referred to as sandmont).

Table 1
Names, abbreviations, organic carbon content, specific surface area, and composition of the model sorbents as well as porosity and bulk density of the respective column packings

Sorbent	Abbreviation	f_{oc} [‰]	Specific surface area	Composition [%]			Column packing	
		$\left[\frac{mg_{oc}}{g_{sorbent}}\right]$	$[\frac{m^2}{g}]$	Sand	PVA	Mont	ϕ $[\frac{cm^3}{cm^3}]$	ρ_b $[\frac{g}{cm^3}]$
Sand	sand	0.29	≤ 0.02[a]	100	–	–	0.41 ± 0.01	1.54 ± 0.05
Sand + PVA	sandPVA	0.61	≤ 0.02[a]	99.9[c]	0.1[c]	–	0.41 ± 0.01	1.56 ± 0.05
Sand + PVA + monmorillonite	sandmont	1.36	10.2[b]	96[c]	0.2[c]	3.8[d]	0.47 ± 0.01	1.39 ± 0.04
Montmorillonite	mont	0.25	267[b]	–	–	100	–	–

[a] Estimated from mean grain size and specific density.
[b] BET measurements.
[c] Calculated from f_{oc} data.
[d] Calculated from specific surface area (BET) data.

The quartz sand (Zimmerli Mineralwerk AG, Zürich, Switzerland) was heated at 550°C for 24 h to remove the organic carbon residues (Deutsche Einheitsverfahren, DEV, DIN, 38409-H1-3, adapted). PVA, or PVA and montmorillonite, respectively, were attached to the quartz sand according to Nakamura et al. (1988): 100 g quartz sand (mean diameter 80–200 μm) was slowly added to suspensions of 0.5 g PVA (Fluka AG, Buchs, Switzerland) in 200 ml water with or without addition of 10 g montmorillonite (Fluka AG) in 50 ml water. The mixtures were boiled until most of the water was evaporated. The resulting sludge was dried at 60°C and sieved (250 μm mesh). Excess clay and PVA were removed by repeated aqueous washings. Fig. 2 shows an enlargement of the obtained particles.

The specific surface of the particles was determined by BET N_2 adsorption (Milestone 100, Carlo Erba Strumentazione, Milano, Italy). Organic carbon content (f_{oc}) was measured with a CHN analyser (CHN-Rapid, Heraeus Instrument, Switzerland). Table 1 summarises some pertinent properties of the sorbents. The dry sorbents were packed into columns and were rinsed excessively with 0.1 M KCl in order to obtain homoionic K^+-clay. As discussed in detail elsewhere (Haderlein and Schwarzenbach, 1993), the presence of weakly hydrated exchangeable cations such as K^+ or NH_4^+ strongly enhances the sorption of nitroaromatic compounds (NACs) to clays.

2.2. Solutes

Table 2 summarises the names, abbreviations and some important properties of the solutes used. All solutes were purchased from Fluka AG in the highest purity available ($\geq 97\%$) and were used as received.

Thiourea was used as a conservative tracer. Although still uncommon in solute transport investigations, this tracer is often used in liquid chromatography due to its hydrophilic properties and the possibility of convenient on-line UV detection (Unger, 1989). In contrast to UV-active ionic tracers such as NO_3^-, neutral thiourea did not

Table 2
Names, abbreviations and some pertinent properties of the tracer solutes (octanol/water partitioning coefficient K_{ow}, acidity constant K_a, wavelength of maximum UV-light absorption λ_{max} and extinction coefficient ε_{max} at λ_{max})

Compound	Abbreviation	log K_{ow}	pK_a	λ_{max} [nm]	ε_{max} [M^{-1} cm^{-1}]
Thiourea	thiourea	−1[a]	1.18[d]	235	1000
4-Methylphenol	*p*-cresol	1.92[b]	10.26[e]	278	1700
4-Sec-butylphenol	psBP	3.72[c]	10.26[e]	222	9200
1,3-Dinitrobenzene	DNB	1.49[a]	–	242	15600

[a] Hansch and Leo, 1979.
[b] Leo et al., 1971.
[c] Values calculated by means of π-fragment constants (Fujita, 1983) and structure factors (Leo et al., 1971).
[d] pK_a of the protonated species ($I = 0.1$ M), Martell and Smith, 1982.
[e] $I = 0.05$ M, Serjeant and Dempsey, 1979.

undergo any significant ion exchange or other sorption processes in our systems. 1,3-Dinitrobenzene (DNB) was chosen as a *model* solute to investigate the effects of nonlinear sorption on solute transport. Under our experimental conditions DNB predominantly adsorbed to the clay fraction of the column matrix exhibiting distinctly nonlinear sorption isotherms. In addition to DNB two hydrophobic tracers that exhibited linear sorption, isotherms were used. *p*-Methylphenol (*p*-cresol, log $K_{ow} \approx 1.9$), which is of similar hydrophobicity as DNB (log $K_{ow} \approx 1.5$), was used to estimate the contribution of hydrophobic partitioning to the overall sorption of DNB. In order to quantify hydrophobic interactions precisely, *p*-sec-butylphenol (psBP, log $K_{ow} \approx 3.7$) was used as a second partitioning tracer.

2.3. Batch experiments

Batch sorption experiments were conducted according to Haderlein and Schwarzenbach (1993) in 1.8 ml-borosilicate glass vials (Omnilab, Mettmenstetten, Switzerland) with aluminium foil liners and septum screw caps (Supelco, Buchs, Switzerland). To exclude cosolvent effects, stock and spike solutions were both prepared in 10 mM aqueous KCl.

A 1 ml solute solution was spiked to 50–600 mg of the dry sorbents. The pH was 5.5 ± 0.5 in all experiments and needed no adjustment. The suspensions were shaken on a rotary shaker for 2–20 h at 22 ± 1.5°C. Phase separation was accomplished by temperature-controlled centrifugation at 12 000 rpm for 2 min. Solute losses during the experimental procedure were hardly significant ($\leq 2\%$) and independent of solute concentration. Blank samples containing spike solutions of solutes but no sorbents were processed in the same way as the suspension samples and were used as external standards. The concentrations of the solutes in the supernatant of each vial were analysed by reversed phase HPLC using a UV-detector at the wavelength of maximum absorption of each analyte (Table 2, injector: Rheodyne 7000i, injection volume 25 μl; column: RP-8 stainless steel cartridges, $4 \cdot 125$ mm, 5 μm-spheres, Merck, Darmstadt, Germany; flow rate: 1 ml min^{-1}; auto sampler: Gina 50, Gynkotek, Germering,

Germany; detector: UVD 340 S, Gynkotek). The mobile phase was a mixture of methanol and water, 60:40 for *p*-cresol and DNB; 70:30 for psBP.

Three sample and blank replicates were run for each concentration step in the sorption isotherms. Individual sorption isotherm points were calculated from triple injections of supernatant according to mass balance considerations. Standard deviations for the sorbed concentrations were calculated based on the error propagation method (Kreyszig, 1979; Sachs, 1982). Coefficients of variation typically were about 3% for strongly sorbing DNB but considerably higher (up to 50%) for weakly sorbing solutes (*p*-cresol, psBP).

2.4. Column experiments

All column experiments were conducted at 22 ± 1.5°C. The experimental set-up is shown in Fig. 3. The solutions from the reservoirs were degassed (on-line degasser: Gastorr GT-104, Omnilab, Switzerland) and were fed to two dual piston HPLC pumps

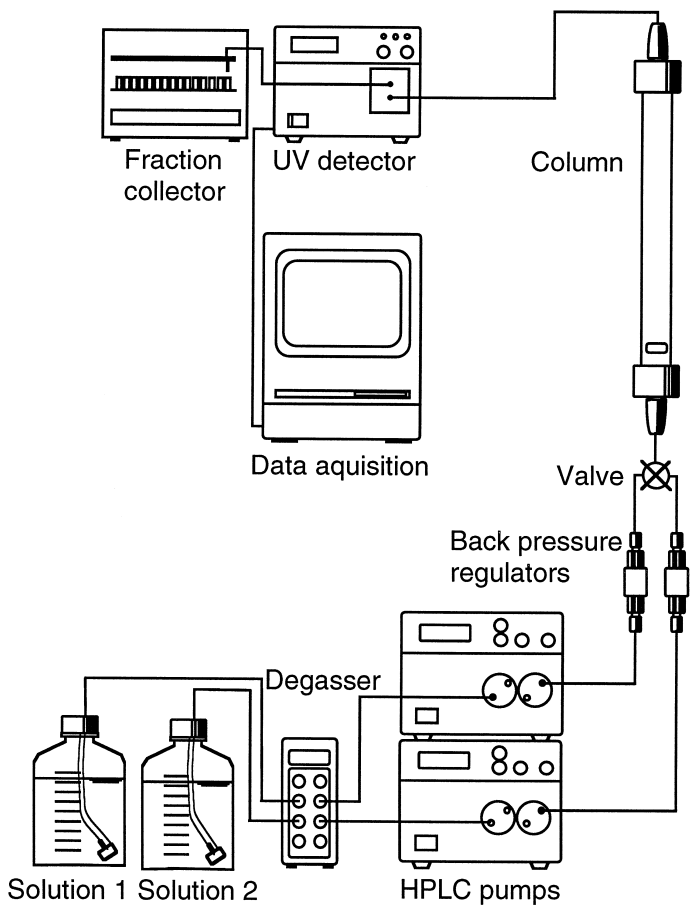

Fig. 3. Experimental set-up for continuous and stopped flow miscible displacement experiments.

(PU 880, Jasco, Japan) equipped with backpressure regulators (Upchurch Scientific, UK). Pore water velocities ranged from 0.03–3 cm min^{-1} and were checked gravimetrically via the outflow. The pumps were connected to the column with a two-way valve (Valco, Switzerland) in order to switch between the solute reservoirs without flow interruption. The column outlet was connected to an UV-vis detector (870-UV, Jasco, Japan) for continuous data acquisition (Workbench, Strawberry Tree, USA). In addition, a fraction collector (Gilson 203B, Gilson, USA) was connected to the detector outlet. In order to obtain an independent measurement of the outflow concentration during long-lasting experiments (more than 1 day) fractions were analysed for solute concentration by HPLC (see above).

Glass columns (i.d. 1.0 cm; length of about 12 cm) with PTFE-end pieces (Omnifit, UK) were equipped with stainless steel frits (pore size 2 μm, Upchurch Scientific) and connected to a stainless steel capillary. Thus, the dead volume of the system (≤ 0.1 ml, corresponding to about 2% of the column pore volume) as well as the contact of the solutes with PTFE was minimised. The columns were packed dry, under continuous tapping against the glass wall as the solid matrix was added. The pore volume and the amount of sorbent were determined gravimetrically. The resulting column porosities, ϕ, and bulk densities, ρ_b, are listed in Table 1.

2.4.1. Continuous flow experiments

Columns were slowly saturated from bottom to top with degassed 10 mM aqueous KCl solution, to minimise gas entrapments, and purged with about 100 pore volumes. Miscible displacement experiments were started by switching to a solution containing 10 mM KCl and the respective solute ($t = 0$). The duration of the solute pulse was adjusted to the type of experiment. Usually, pulses of about two pore volumes were chosen for the conservative and the hydrophobic tracers, and 40–160 pore volumes for DNB. Solute concentrations were always within the linear range of the UV-vis detector. Table 3 summarises the experimental conditions of all continuous flow column experiments.

Mass balances of all solutes ranged from 97–101% indicating that losses of the solutes (e.g., due to biological or chemical transformations or irreversible sorption) were negligible.

2.4.2. Interrupted flow experiments

A set of interrupted flow experiments was performed in order to discriminate between dispersion and nonequilibrium effects. During flow interruption solute transport proceeds only by diffusion. Changes in aqueous solute concentrations with increasing periods of flow interruption may be used to identify and quantify processes such as intra-aggregate diffusion (Murali and Aylmore, 1980; Brusseau et al., 1989; Koch and Fluehler, 1993; Brusseau et al., 1997). Interrupted flow experiments with multiple tracers may even facilitate an assessment of the accessibility of reactive sorption sites at the pore scale of the column packing.

Interrupted flow experiments were conducted similarly to the continuous flow experiments except for periods of flow interruption in the leading and tailing fronts of the BTCs. The pump was stopped for time intervals equivalent to about 2 to 36 pore volumes of continuous flow.

Table 3
Summary of the experimental conditions and the data analysis of the continuous flow column studies

Solute[a]	Sorbent[b]	Relevant processes	Program used for data analysis	Parameters to be calculated	Flow velocities [cm min^{-1}]	C_0 [μmol l^{-1}]	Pulse length (pore volumes)
Thiourea	sand						
	sandPVA	advection (A), dispersion (D)	CXTFIT	*D* (Table 5)	3.0/0.3/0.03	60	2.2
	sandmont						
p-Cresol	sand						
	sandPVA	A, D, *linear* sorption	CXTFIT	*R* (Table 6)	3.0/0.3/0.03	200	2.2
	sandmont						
psBP	sand						
	sandPVA	A, D, *linear* sorption	CXTFIT	*R* (Table 6)	3.0/0.3/0.03	100	2.2
	sandmont						
DNB	sand						
	sandPVA	A, D, *linear* sorption	CXTFIT	*R* (Table 6)	3.0/0.3/0.03	50	2.2
	sandmont	A, D, *nonlinear* sorption;	AQUASIM	see Tables 6 and 7	3.0/0.3/0.03	50	57/57/44
		mobile/immobile mass transfers			3.0	50/12.5/2	57/57/160

[a] See Table 1.
[b] See Table 2.

2.4.3. Incremental in situ adsorption isotherms

An incremental method according to Schweich and Sardin (1981) was used to determine adsorption isotherms of NACs from BTCs. Such in situ isotherms can be compared to batch isotherms in order to compare the relative fraction of accessible sorption sites in both systems. The in situ method used is based on the integration of the adsorption fronts of a series of solute pulses. Stepwise, the solute concentration was instantaneously increased from C_n to C_{n+1}. The sorbed-phase solute concentration, $S(C)$, of each step was calculated according to:

$$C_{n+1} - C_n + \frac{\rho_b}{\theta}\left[S(C_{n+1}) - S(C_n)\right] = \frac{1}{t_0}\int_{t_{n,n+1}}^{\infty}\left[C_{n+1} - C(t)\right]dt. \quad (1)$$

For definitions of the parameters, see Section 5. The integral is equivalent to the area between the increasing branch and the concentration C_{n+1} of the BTC (Fig. 4b). It is

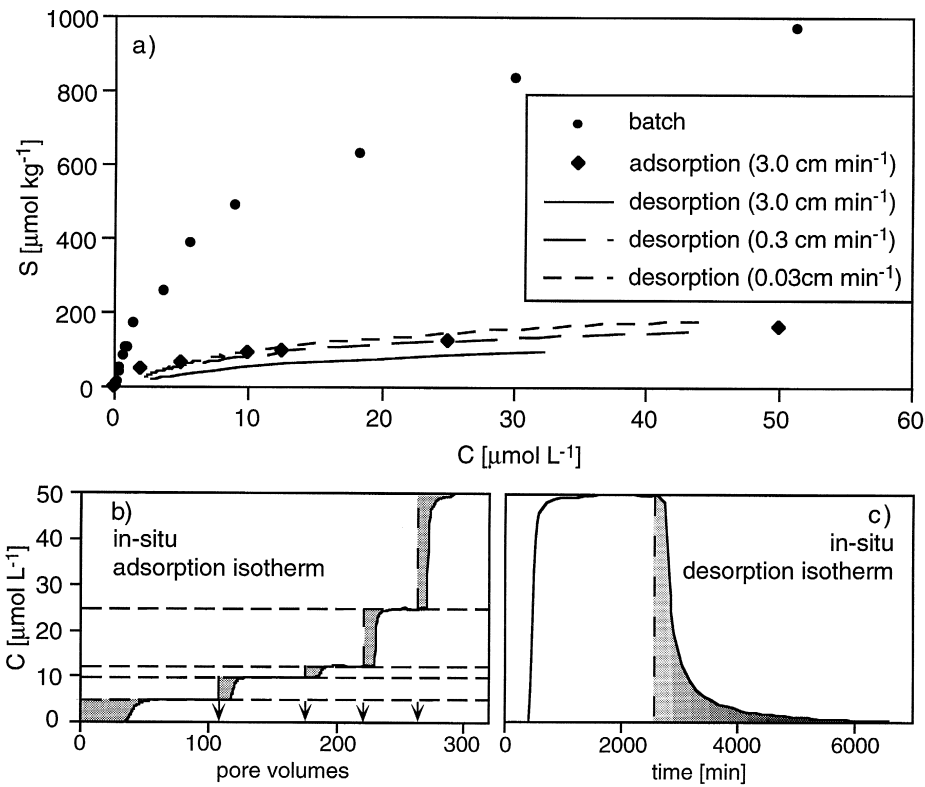

Fig. 4. (a) Comparison of Langmuir–Freundlich type sorption isotherms of DNB at clay coated quartz sand as determined by batch adsorption and two types of in situ methods (Eq. (1)). In all experiments, the same isotherm parameter values $\alpha = 0.57$ and $K_{LF} = 0.12\ l^{0.57}\ \mu mol^{-0.57}$ were obtained while S_{max} varied between the different systems: S_{max} (batch) = 1792 μmol kg^{-1}, S_{max} (in situ adsorption) = 300 μmol kg^{-1}, S_{max}(desorption 3.0 cm min^{-1}) = 187 μmol kg^{-1}, S_{max}(desorption 0.3 cm min^{-1}) = 265 μmol kg^{-1}, S_{max} (desorption 0.03 cm min^{-1}) = 306 μmol kg^{-1}. (b) and (c) Illustration of the integration procedures to calculate in situ isotherms. The shaded areas represent the amount of sorbed DNB.

essential that a steady state concentration of the solutes is reached prior to performing a new concentration step. The incremental method was performed in five concentration steps of DNB in the column packed with sandmont.

Additionally, in situ isotherms of DNB were obtained by integrating the desorption front of one concentration pulse (Aris and Amundson, 1973; Schweich and Sardin, 1981; Bürgisser et al., 1993). Starting from the end of the BTC where the solute concentration was below the detection limit, the area under the BTC was numerically integrated resulting in one point of the desorption isotherm for each discretisation step (Fig. 4c). In contrast to the adsorption isotherm obtained with the incremental method, effects of slow desorption kinetics are inherent in this isotherm.

2.5. Data analysis and modeling

BTCs of the conservative and hydrophobic tracers were analysed with the computer code CXTFIT (Parker and van Genuchten, 1984; Toride et al., 1995) that uses an analytical solution of the one-dimensional advective dispersive transport equation including exchange with an immobile region and linear sorption. This allowed to estimate parameter values of the hydrodynamic dispersion coefficient, D, and the retardation factor, R, very efficiently and precisely. For linearly sorbing solutes, R was fitted with the aid of measured BTCs using D obtained from thiourea breakthrough data.

Unfortunately, analytical solutions are not available for transport equations of nonlinearly sorbing solutes. Therefore, the BTCs of the nonlinearly sorbing DNB in the column containing sandmont were analysed numerically with the simulation and data analysis program AQUASIM (Reichert, 1994; Reichert, 1995) which was extended to cover one-dimensional solute transport in porous media (Simon and Reichert, 1997). The average retardation factors, R, of these asymmetric BTCs were calculated by integration of the adsorption fronts. Table 3 indicates which data analysis scheme was used in the various continuous flow experiments. Note that very similar results were obtained when AQUASIM was used instead of CXTFIT to analyse the BTCs of the conservative and hydrophobic tracers. However, the computational effort was much higher with AQUASIM because of its use of a numerical integration technique. Interrupted flow experiments were generally analysed with AQUASIM since CXTFIT does not offer this possibility. With AQUASIM, advective dispersive solute transport can be coupled to various types of exchange processes with the immobile regions. Any type of chemical processes such as linear and/or nonlinear sorption can be specified by the user.

For parameter estimation, the weighted deviations between measured and simulated concentration time series at the column outlet, χ^2, were minimised:

$$\chi^2 = \sum_{i=1}^{n} \left(\frac{C_{\mathrm{meas},i}(L,t_i) - C_{\mathrm{calc}}(L,t_i)}{\sigma_{\mathrm{meas},i}} \right)^2 . \qquad (2)$$

This procedure assumes that the concentration measurements contain errors while the time axis is known precisely. However, in reality, the error associated with the experimental determination of the pore volume is propagated to the breakthrough time.

Table 4
Estimated standard deviations for the aqueous solute concentration, C, and the time, t, of measured breakthrough curves at different solute input concentrations and pore water velocities

Pore water velocity [cm min^{-1}]	Input concentration [μmol l^{-1}]	σ^{a}_{conc} [μmol l^{-1}]	σ^{b}_{time} [min]
3.0	50	0.5	0.5
3.0	12.5	0.4	0.5
3.0	2	0.2	0.5
0.3	50	0.5	5
0.03	50	1	70

[a] σ_{conc} was estimated according to the precision of the on-line UV-detector, which decreased with absolute solute concentration and prolonged duration of the experiments.
[b] σ_{time} was estimated according to the independent flow measurements (Section 2.4).

In the case of steep slopes of BTC fronts, even a small error in the breakthrough time causes a very large deviation in the front concentrations. In order to account for this effect, for the data evaluations performed with AQUASIM the standard deviations, $\sigma_{meas,i}$, used in Eq. (2) were individually calculated as follows:

$$\sigma_{meas,i} = \sqrt{\sigma_{conc}^2 + \Gamma_i^2 \sigma_{time}^2} \quad i = 1, \ldots, n \tag{3}$$

where Γ_i is a smoothed value of the slope of the measured BTCs at the measurement i. The standard deviations σ_{conc} and σ_{time} varied with pore water velocity and inlet concentration. Estimated values of these deviations are given in Table 4. This technique of calculating the standard deviations significantly improved convergence of the parameter estimation algorithm. The parameter estimates, however, where not very sensitive to variations in σ_{time}. For the data evaluations with CXTFIT a constant (and therefore, irrelevant) value of $\sigma_{meas,i}$ was used. A convergence problem of the fit algorithm did not occur in this case probably due to the smaller number of estimated parameters and the less steep concentration fronts for the linearly sorbing solutes.

The following numerical algorithms were used: in a first step, partial differential equations were discretised in space using a high resolution flux-limiter scheme to avoid numerical diffusion (van Leer, 1974; LeVeque, 1990). The Gear algorithm implemented by Petzold (1983) was then used to integrate the system of ordinary differential and algebraic equations in time (method of lines). For minimising χ^2 according to Eq. (2) the simplex algorithm by Nelder and Mead (1965) and the secant algorithm by Ralston and Jennrich (1978) were used consecutively in order to improve convergence.

3. Results and Discussion

3.1. BTCs of conservative tracer and hydrodynamic properties of the columns

The hydrodynamic properties of the three columns packed with the three different sorbents were inferred from BTCs of the conservative tracer thiourea (Fig. 5a). The normalised BTCs were equal at different flow velocities. The shape of the BTCs was

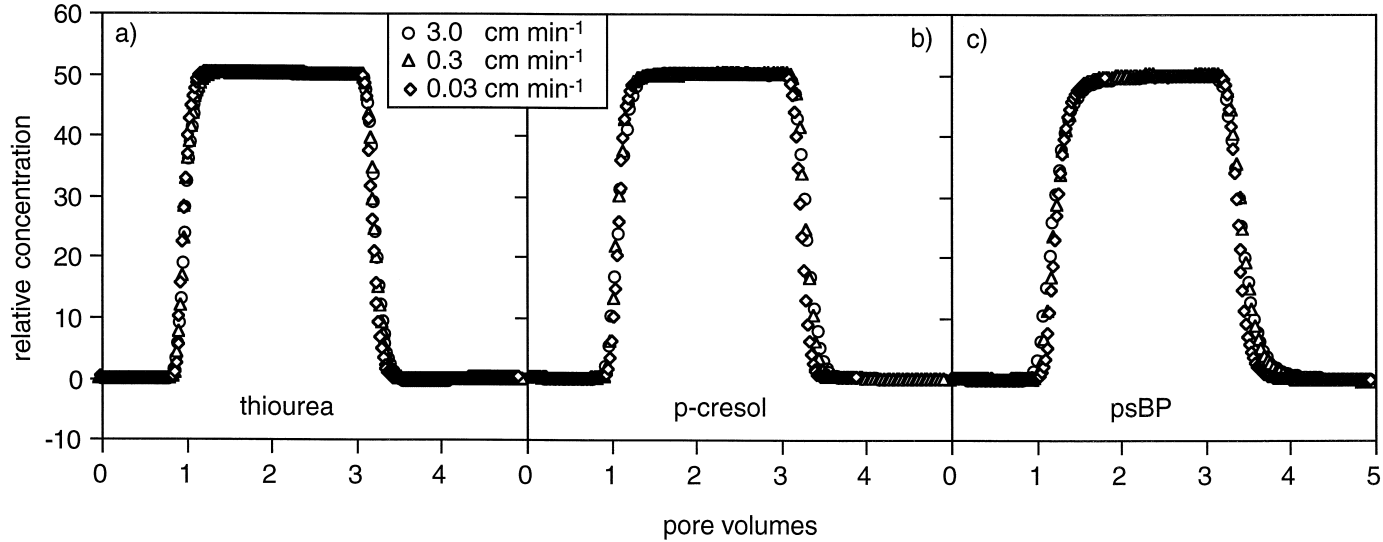

Fig. 5. Effect of pore water velocity on BTCs of the conservative tracer (thiourea) and the hydrophobic partitioning tracers (*p*-cresol and psBP) in a column packed with clay coated sand. BTCs of these tracers measured in the sand and sand PVA column exhibit very similar features.

Table 5
Hydrodynamic properties of the three types of packed columns used

Sorbent	Flow velocity, [cm min^{-1}]	Dispersion coefficient, D [cm^2 min^{-1}]	Dispersivity λ [μm]
Sand	0.03	0.00086 ± 0.0002	291 ± 64
	0.3	0.0048 ± 0.0005	159 ± 16
	3.0	0.057 ± 0.003	185 ± 11
SandPVA	0.03	0.00072 ± 0.00001	210 ± 21
	0.3	0.0084 ± 0.0003	266 ± 11
	3.0	0.120 ± 0.005	381 ± 15
Sandmont	0.03	0.00077 ± 0.00001	301 ± 48
	0.3	0.0068 ± 0.0004	254 ± 13
	3.0	0.100 ± 0.006	369 ± 22

highly symmetric with sharp fronts and breakthrough after exactly one pore volume. All data were well described by the one-dimensional advection dispersion equation (ADE), introduced by Lapidus and Amundson (1952):

$$\frac{\partial C}{\partial t} = D\frac{\partial^2 C}{\partial x^2} - \nu\frac{\partial C}{\partial x}. \tag{4}$$

The hydraulic dispersivities ($\lambda = D/v$) of the three types of packed columns ranged between 160 and 380 μm (Table 5), comparable to the grain size of the column matrix. The corresponding column Peclet numbers, $\mathrm{Pe} = \frac{v \cdot L}{D}$, ranged between 800 and 320. The results indicate that the flow regime within all columns studied was dominated by advection which allowed to neglect dispersion effects in the modeling of BTCs of the reactive tracers (Schweich and Sardin, 1981; Brusseau and Rao, 1989). Furthermore, immobile or stagnant regions within the columns, if present at all, apparently were not significant for the transport of the conservative tracer. This was corroborated by the fact that no measurable changes in aqueous concentrations of thiourea were observed during flow interruption experiments (data not shown). A comparison of the tracer breakthrough volume with the gravimetrically measured column pore volume revealed that the fraction of immobile regions was less than 1% of the total column pore volume.

3.2. Sorption and transport of reactive tracers

To analyse the BTCs of sorbing solutes the isotherm equation was substituted into the ADE (Eq. (4)) yielding

$$\frac{\partial C}{\partial t} = \frac{D}{R}\frac{\partial^2 C}{\partial x^2} - \frac{\nu}{R}\frac{\partial C}{\partial x} \tag{5}$$

with the retardation factor

$$R = 1 + \frac{\rho_b}{\theta}\frac{\mathrm{d}S}{\mathrm{d}C}. \tag{6}$$

Table 6 gives an overview of the results of sorption and retardation parameters of all reactive tracers in the various systems.

Table 6
Calculated retardation factors (R) and adsorption coefficients (K_d) of reactive tracers in the three model columns and K_d values measured in batch sorption experiments

Sorbent	Pore water velocity [cm min^{-1}]	4-Methylphenol			4-sec-Butylphenol			1,3-Dinitrobenzene		
		R [−]	K_d column [l kg^{-1}]	K_d batch [l kg^{-1}]	R [−]	K_d column [l kg^{-1}]	K_d batch [l kg^{-1}]	R [−]	K_d column [l kg^{-1}]	K_d batch [l kg^{-1}]
Sand	0.03	1.036 ± 0.001	0.010		1.099 ± 0.001	0.027		1.261 ± 0.005	0.033	
	0.30	1.005 ± 0.001	0.002	0.01 ± 0.01	1.040 ± 0.001	0.011	0.04 ± 0.04	1.143 ± 0.006	0.038	0.09 ± 0.03
	3.00	1.015 ± 0.001	0.004		1.040 ± 0.002	0.011		1.125 ± 0.021	0.070	
SandPVA	0.03	1.016 ± 0.001	0.004		1.122 ± 0.007	0.032		1.275 ± 0.020	0.071	
	0.30	1.013 ± 0.001	0.003	0.01 ± 0.01	1.099 ± 0.002	0.026	0.04 ± 0.02	1.074 ± 0.004	0.019	0.05 ± 0.03
	3.00	1.013 ± 0.001	0.003		1.108 ± 0.026	0.028		1.037 ± 0.003	0.010	
Sandmont	0.03	1.063 ± 0.001	0.021		1.248 ± 0.084	0.084		16.85[a]	5.35[a]	135(2 μM)[c]
	0.30	1.055 ± 0.001	0.019	0.05 ± 0.02	1.234 ± 0.004	0.079	0.11 ± 0.07	12.95[a]	4.03[b]	48(12.5 μM)[c]
	3.00	1.065 ± 0.002	0.022		1.205 ± 0.005	0.069		10.44[a]	3.52[b]	19(50 μM)[c]

[a]Average R for $C_0 = 50$ μM; due to sorption isotherm nonlinearity R is strongly dependent on DNB concentrations.[b]K_d-values calculated from average R for $C_0 = 50$ μM (switch from $C = 0$ μM),[c]K_d-value for typical solute concentrations, C_w, (values given in parenthesis); due to sorption isotherm nonlinearity K_d-values increase with decreasing concentration of DNB.

3.2.1. Linearly sorbing (hydrophobic) tracers

As can be seen in Fig. 5b and Table 6, sorption and retardation of the hydrophobic tracer *p*-cresol was very low in all systems and at all conditions studied. The BTCs were symmetric and interrupted flow experiments did not show any measurable change of aqueous solute concentrations during flow interruption (data not shown). Also, the retardation factors were very similar for different pore water velocities. This indicates that diffusion into organic matter did not cause significant nonequilibrium effects on the time scales considered. The batch isotherms of the hydrophobic tracers *p*-cresol and psBP were linear with very low slopes ($K_d \leq 0.1$ l kg^{-1}). As physical nonequilibrium effects could be neglected, K_d values of linear batch isotherms relate directly to the retardation factors of the BTCs (e.g., see the work of Brusseau, 1994)

$$R = 1 + \frac{\rho_b}{\theta} K_d \tag{7}$$

The K_d-values obtained from the retardation of the BTCs were in the same range as the respective batch values. The affinity of both hydrophobic tracers increased slightly with increasing fractions of organic matter (PVA) present in the solid matrix. Sorption and retardation of the more hydrophobic tracer psBP was slightly higher compared to *p*-cresol. However, the retardation factors were 1.25 at most. The results indicate that hydrophobic interactions cause only minor retardation of the compounds of interest within the systems studied. The symmetric BTCs suggest that local equilibrium conditions apply for hydrophobic partitioning within the columns.

Since *p*-cresol and DNB exhibit very similar hydrophobicities, the batch equilibrium sorption of DNB to quartz sand and sandPVA was very weak and linear with $K_d \leq 0.1$ l kg^{-1} (Table 6). Consistently, DNB was only slightly retarded in miscible displacement experiments in the absence of montmorillonite (Table 6). However, the retardation increased with slower pore water velocities (R ranging from 1.04 to 1.28). The BTCs (not shown) were almost symmetric but exhibited a slight tailing in both the adsorption and the desorption front. The slight tailing of the BTCs was consistent with a weak but somewhat nonequilibrium sorption process, which was supported by the fact, that the retardation increased with decreasing pore water velocities. However, these minor interactions due to hydrophobic partitioning are negligible compared to the very strong retardation of DNB in columns containing clay minerals (see below).

3.2.2. Nonlinearly sorbing tracer

While sorption of DNB to quartz sand and sandPVA was low and linear, sandmont had a high affinity and DNB exhibited a distinctly nonlinear, saturation type sorption isotherm (Fig. 4a). These features are typical for complex formation of NACs with clay minerals (Haderlein et al., 1996; Weissmahr et al., 1998). The sorption behaviour could be described best with a Langmuir–Freundlich isotherm (Kinniburgh, 1986):

$$S(C) = S_{max} \frac{K_{LF} C^{\alpha}}{1 + K_{LF} C^{\alpha}}. \tag{8}$$

Fitting two-parametric isotherms (i.e., Langmuir or Freundlich) to the data resulted in significant deviation either at low or high concentrations (not shown).

In addition to the batch isotherm, a sorption isotherm of DNB for sandmont was determined within the column system (see Section 2). Fig. 4b shows BTCs that resulted from a stepwise increased DNB input concentration. The resulting adsorption isotherm data was also fitted best with the Langmuir–Freundlich equation. Fig. 4a shows that in batch experiments the sorption capacity of sandmont for DNB was considerably higher than in column experiments (S_{max} (batch) $\approx 6 \cdot S_{max}$ (column)). Higher sorption in batch experiments may be due to an increase of accessible clay surface area resulting from disaggregation of clay clusters during shaking and/or from abrasion processes. Alternative explanations include a loss of clay minerals during the initial conditioning of the column or a limited accessibility of clay sorption sites in the column due to dense packing. All these processes potentially result in sorption isotherms of similar shape but different sorption capacities as observed in our experiments. However, the present data do not allow to unambiguously distinguish between such processes in our system.

*De*sorption isotherms of DNB in the column were calculated from the desorption fronts of the BTCs for the three different pore water velocities (Fig. 4c). The apparent maximum of these isotherms increased with decreasing pore water velocity. At the highest flow rate, the slopes of the isotherm of the desorption experiment were much smaller than that of the adsorption experiment where steady-state conditions were reached. In contrast, the two desorption isotherms obtained at lower flow rates were comparable to the in situ adsorption isotherm indicating that in these experiments the major fraction of the totally available sorption sites were accessible.

Generally, DNB was strongly retarded in the column packed with sandmont (Fig. 6, Table 6). The BTCs exhibited sharp adsorption fronts and strong tailing at the desorption fronts consistent with nonlinear, saturation type isotherms. Experiments conducted at different input concentrations showed decreasing retardation of the breakthrough of DNB with increasing solute concentrations (Fig. 6b) as expected for solutes exhibiting saturation type isotherms (Schweich and Sardin, 1981; Bürgisser et al., 1993). The tailing of the adsorption fronts (Fig. 6a), which became more evident at low pore water velocities, indicated the presence of nonequilibrium processes. This was supported by the results of interrupted flow experiments (Fig. 6c). The change in aqueous DNB concentrations in the columns was higher the longer the flow was interrupted. During flow interruption, the aqueous concentration of DNB decreased in the adsorption fronts but increased in the desorption fronts of the BTCs. Finally, the presence of nonequilibrium processes was also indicated by an increased retardation of DNB with decreasing pore water velocity (Fig. 6a). Consistent with these results, the fronts of the BTCs were less sharp than predicted by a one-region transport model based on the ADE (Eq. (4)) including nonlinear sorption and assuming equilibrium conditions (data not shown).

3.3. Modeling of nonlinear sorption and nonequilibrium solute transport in aggregated porous media

As discussed earlier, nonequilibrium effects in solute transport may be due to various different processes. The results of our experiments using conservative and hydrophobic tracers imply that, for the systems studied in this work, the fraction of immobile regions was rather small and intra-organic matter diffusion negligible. Chemical nonequilibrium

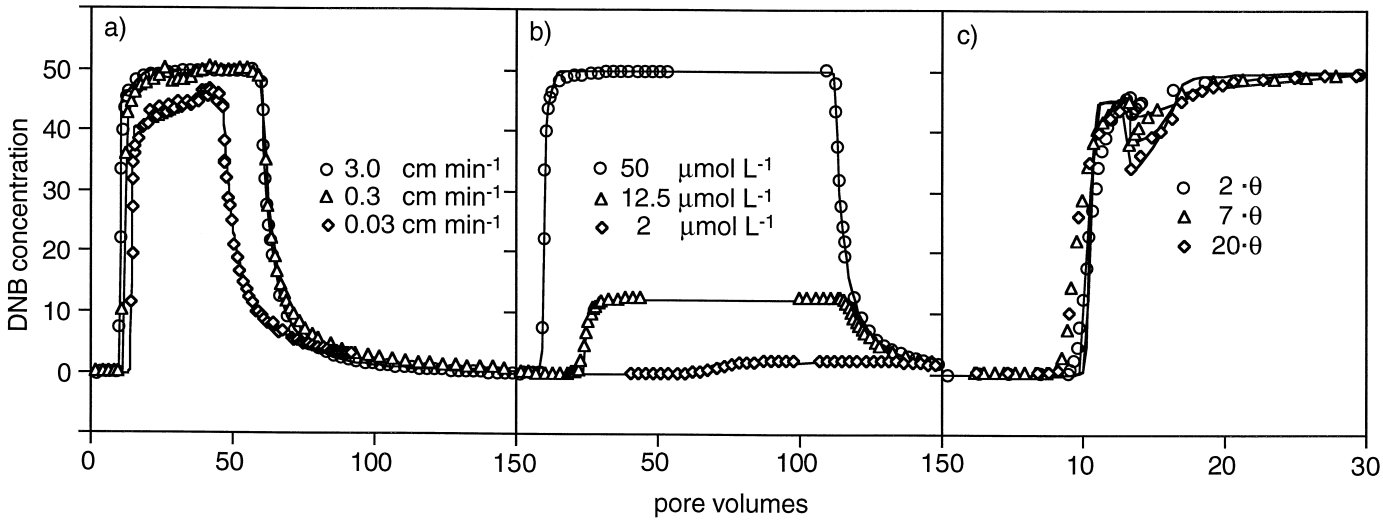

Fig. 6. BTCs of DNB in a column containing clay coated sand matrix. Markers represent measured data, lines show fits obtained with a classic two-region model (Section 3.3.1; see Table 7 for parameter values) that assumes homogeneous solute concentrations within the clay aggregates. (a) At decreasing pore water velocities, v, the retardation and the asymmetry of the BTCs increased ($C_0 = 50$ μmol l^{-1}). (b) At decreasing inlet concentrations, C_0, the retardation of the adsorption front increased due to the convexly shaped sorption isotherm ($v = 3.0$ cm min^{-1}). (c) With prolonged periods of flow interruption the change in 1,3-DNB concentration became more distinct (interruption periods are given in the units of volumetric water content, θ, corresponding to the volume of liquid that would have been pumped through the column at steady flow) ($v = 3.0$ cm min^{-1}; $C_0 = 50$ μmol l^{-1}). Note the different scales of the abscissa.

due to rate-limited sorption can be ruled out since sorption of NACs to clay minerals proceeds quasi instantaneously under batch conditions where the sorption sites are easily accessible (Haderlein et al., 1996). Pore scale variation in retardation factor, as recently proposed (Sugita and Gillham, 1995a,b; Sugita et al., 1995), is not sufficient to account for the effects observed in our experiments since such pore scale variation in retardation factor leads to tailing of BTCs but not to the nonequilibrium behaviour observed in the interrupted flow experiments.

Thus, the data suggest that retarded intra-aggregate diffusion of DNB is the major process contributing to the observed nonequilibrium effects. As is conceivable by inspection of Figs. 1 and 2, a certain fraction of the pores within the clay aggregates may only be accessible by diffusion. Although such immobile regions within the clay aggregates represent only a very small fraction of the total pore volume of the columns ($< 1\%$, see Section 3.1), they could host a significant fraction of the sorption sites for NACs.

To simulate the data, two two-region models were tested that assumed a mobile region dominated by advective flow and an immobile region reached by diffusion only (see below). The total porosity of the column, ϕ, is the sum of the porosity of the mobile region, ϕ_{mob}, and that of the immobile region, ϕ_{im}:

$$\phi = \phi_{mob} + \phi_{im} \tag{9}$$

where ϕ_{im} is given as:

$$\phi_{im} = f_{im} \cdot \phi \tag{10}$$

and f_{im} is the fraction of the immobile region of the total porosity.

3.3.1. Two region model with homogeneous solute concentration within aggregates

In a first approach, a classical two-region model was used. In this model, it is assumed that both regions are completely mixed in lateral direction and that nonlinear equilibrium sorption takes place. Based on the results presented in Section 3.1, the porosity of the immobile region was set to be $\phi_{im} = 0.001 \cdot \phi$, i.e., 1‰ of the total porosity. The size of the immobile region cannot be determined from the data since its storage capacity is determined by the sorption sites and not by the volume. The total solute concentrations expressed as total mass of solute per liquid volume are then given by:

$$C_{mob}^{tot} = C_{mob} + \frac{\rho_b}{\theta_{mob}} S_{mob} \tag{11}$$

$$C_{im}^{tot} = C_{im} + \frac{\rho_b}{\theta_{im}} S_{im} \tag{12}$$

where the sorbed-phase solute concentrations, S, can be calculated from the aqueous concentration using a nonlinear isotherm, in this case Langmuir–Freundlich type (Eq. (8)):

$$S_{mob}(C_{mob}) = S_{max,mob} \frac{K_{LF} C_{mob}^{\alpha}}{1 + K_{LF} C_{mob}^{\alpha}} \tag{13}$$

$$S_{im}(C_{im}) = S_{max,im}\frac{K_{LF}C_{im}^{\alpha}}{1+K_{LF}C_{im}^{\alpha}} \quad (14)$$

The maximal sorbed phase solute concentration, S_{max} may be different in the mobile and immobile regions reflecting the distribution of sorption sites in contact with the respective region. The exchange between the two regions is described with a first-order mass transfer coefficient, k_{ex}. Thus, the advective dispersive transport in the mobile region and the mass exchange with the immobile region are given as:

$$\frac{\partial C_{mob}^{tot}}{\partial t} = -\nu\frac{\partial C_{mob}}{\partial x} + D\frac{\partial^2 C_{mob}}{\partial x^2} - \frac{k_{ex}}{\theta_{mob}}(C_{mob} - C_{im}) \quad (15)$$

$$\frac{\partial C_{im}^{tot}}{\partial t} = \frac{k_{ex}}{\theta_{im}}(C_{mob} - C_{im}). \quad (16)$$

To model the BTCs of DNB in our system, the respective hydrodynamic and column parameter values determined in independent experiments (see Section 3.1) were used. Moreover the values K_{LF} and α of the Langmuir–Freundlich isotherm were determined independently and assumed to be constant (compare to Fig. 4, legend). The parameter values of the mass transfer coefficient, k_{ex}, and the maximum sorbed-phase solute concentrations, $S_{max,\,mob}$ and $S_{max,\,im}$ were fitted to the data of all five continuous flow column experiments conducted at different flow velocities and DNB input concentrations (Table 3). The data of the three interrupted flow experiments were simulated with the resulting parameter values. Note that in our case S_{max} is equivalent to the density of sorption sites at the solid matrix within the respective region. Due to the accumulation of clay minerals within the aggregates (see Fig. 2) a fraction of 12 to 32% of the total accessible sorption sites was located in the immobile regions despite their very low volumetric fraction ($< 1\%$) (see Table 7). The parameter values optimised for the various experimental conditions are given in Table 7. As can be seen in Fig. 6, the BTCs of DNB obtained at various flow rates could be fitted quite well with this model using the respective sets of parameter values. However, in order to obtain a good agreement of measured and fitted BTCs under different flow conditions, different parameter values of both, $S_{max,\,im}$ and k_{ex} were necessary. Note that this classical two-region model assumes a homogeneous distribution of solutes within the immobile regions and thus does not consider concentration gradients due to (retarded) diffusion within aggregates. The resulting parameter values of $S_{max,\,mob}$ and $S_{max,\,im}$ increased with decreasing pore water

Table 7
Parameter values fitted for the transport of -DNB by a classic two-region model which assumes homogeneous solute concentrations within the clay aggregates

Pore water velocity [cm min^{-1}]	$S_{max,\,mob}$ [μmol kg^{-1}]	$S_{max,\,im}$ [μmol kg^{-1}]	k_{ex} [min^{-1}]	χ^2
3.0	253	51	0.041	80
0.3	329	45	0.0011	181
0.03	352	170	0.00016	88

Different pore water velocities resulted in different sets of parameter values.

velocities (Table 7). Such phenomena were also studied recently by (Hu and Brusseau, 1996) who reported a 'rate-limited sorption process' due to diffusion of herbicides into/out of components of the sorbent. They also determined exchange coefficients and fractions of sorbent in each region that varied with pore water velocity. A more detailed discussion of the effects of pore water velocity on parameter values of first order rate constants in such models can be found in the works of Rao et al. (1980), Young and Ball (1995) and Bajracharya and Barry (1997).

Since a simultaneous fit of experiments at different flow velocities with one set of parameter values was impossible (not shown), the classical two-region model used cannot be considered as a meaningful physical model for describing the transport of reactive solutes that sorb strongly to sites that are accumulated within immobile regions of a porous medium. Our results show that the amount of sorption sites in the mobile region, $S_{\mathrm{max,\ mob}}$ and the mass transfer coefficient, k_{ex}, depended on the pore water velocity. The pore water velocity determines the time period available for diffusion of solutes into the aggregates during the steep concentration increase of the adsorption front of the BTC. The penetration of solutes into the immobile regions during this time affects the shape of the adsorption front. This explains the decreasing values of k_{ex} and the increasing values of S_{max} for different pore water velocities. Thus, to overcome these shortcomings, a model is necessary that more accurately describes diffusion processes of the solutes within the aggregates.

3.3.2. Two-region model with retarded solute diffusion within aggregates

A model was therefore developed that, in contrast to the simple two-region model described above, is able to resolve the spatial distribution of solutes within the aggregates due to retarded diffusion processes. Using Fick's first law of diffusion, the diffusive flux within the immobile regions, F_{im}, is given as:

$$F_{\mathrm{im}}(z) = -a(z)\,D_0\frac{\partial C_{\mathrm{im}}}{\partial z}(z) \tag{17}$$

where $a(z)$ is the sum of the cross-sectional areas of all pores building the immobile region per unit column volume. It is measured perpendicular to the direction of diffusion into the pores and may vary with the spatial coordinate along the pores, z. The volumetric water content of the immobile region is given as:

$$\theta_{\mathrm{im}} = \int_0^d a(z)\,\mathrm{d}z \tag{18}$$

where d is the maximal length of the pores of the immobile region. The sorbed-phase solute concentration is given as:

$$S_{\mathrm{im}} = \int_0^d s_{\mathrm{im}}(z)\,\mathrm{d}z \tag{19}$$

with $s_{\mathrm{im}}(z)$ being the sorbed-phase solute concentration per unit pore depth, z, of the immobile region, leading to the following total solute concentration in the depth z:

$$C_{\mathrm{im}}^{\mathrm{tot}}(z) = C_{\mathrm{im}}(z) + \frac{\rho_{\mathrm{b}}}{a(z)}s_{\mathrm{im}}(z). \tag{20}$$

The transport equations in the mobile and immobile regions, respectively, can then be written as follows:

$$\frac{\partial C_{\mathrm{mob}}^{\mathrm{tot}}}{\partial t} = -\nu\frac{\partial C_{\mathrm{mob}}}{\partial x} + D\frac{\partial^2 C_{\mathrm{mob}}}{\partial x^2} - \frac{F_{\mathrm{im}}(0)}{\theta_{\mathrm{mob}}} \tag{21}$$

$$\frac{\partial C_{\mathrm{im}}^{\mathrm{tot}}}{\partial t} = \frac{1}{a(z)}\frac{\partial}{\partial z}\left(a(z)D_0\frac{\partial C_{\mathrm{im}}}{\partial z}\right). \tag{22}$$

With the boundary conditions:

$$C_{\mathrm{im}}(0) = C_{\mathrm{mob}} \tag{23}$$

$$\frac{\partial C_{\mathrm{im}}}{\partial z}(d) = 0. \tag{24}$$

Again, the sorbed-phase concentrations were calculated by Eqs. (13) and (14) with K_{LF} and α as determined from the independent series of column experiments. The maximum sorbed-phase solute concentration in the immobile region, $s_{\mathrm{max,\ im}}$, can be a function of the spatial coordinate along the pores z (see below). The model is an extension of the diffusion models as presented by, e.g., the works of Glueckauf and Coates (1947) and Wu and Gschwend (1986), who assumed a radial geometry of the immobile regions, to nonlinear sorption and an arbitrary geometry of the immobile regions with an arbitrary distribution of sorption sites over the pore depth.

In order to implement this continuous model numerically, the immobile region within the aggregates was discretised into n zones (Fig. 7). This discretised version of the continuous model is similar to the multiple-rate mass transfer model of Haggerty and Gorelick (1995). In contrast to their assumption of parallel zones with different diffusion rates, we obtain a serial arrangement and nonlinear processes may be included.

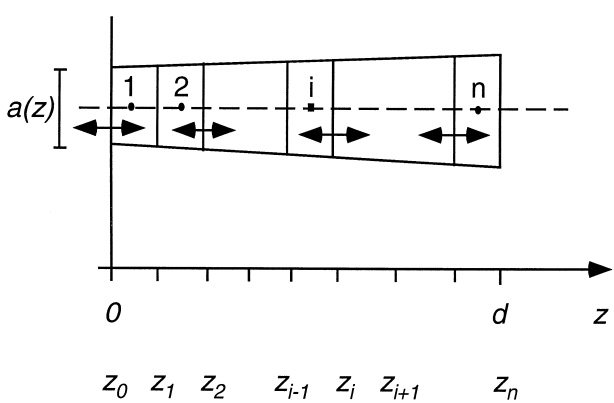

Fig. 7. Schematic representation of various zones ($0 \le i \le n$) within the immobile regions (i.e., the clay aggregates). $a(z)$ represents the cross-sectional area of the pores per unit column volume, z_i denotes the spatial coordinates of the boundaries between the single discretised zones, and d is the maximal length of the pores.

However, the large number of parameters used by Haggerty and Gorelick (1995) was reduced in our model by using algebraic functions to describe $a(z)$ and $s_{\max,\,\mathrm{im}}(z)$ (see below).

In the discretised version of the model, the immobile water content is given as:

$$\theta_{\mathrm{im}} = \sum_{i=1}^{n} \theta_{\mathrm{im},i} \tag{25}$$

the volumetric water content of each zone being:

$$\theta_{\mathrm{im},i} = \int_{i=1}^{z_i} a(z)\,\mathrm{d}z. \tag{26}$$

For a numerical approximation the trapezoidal rule results in:

$$\theta_{\mathrm{im},i} \approx \frac{(a(z_i) + a(z_{i-1}))(z_i - z_{i-1})}{2} \tag{27}$$

where z_i $(i = 0,\ldots,n;\ z_0 = 0,\ z_n = d)$ denotes the boundary between zones. The mass transfer between the mobile region and the first zone can be approximated as:

$$F_{\mathrm{im}}^{1} = -a(0)\,D_0 \frac{C_{\mathrm{im},1} - C_{\mathrm{mob}}}{\frac{z_1}{2}} \tag{28}$$

the transfer between zone $i-1$ and zone i as:

$$F_{\mathrm{im}}^{i} = -a(z_{i-1})\,D_0 \frac{C_{\mathrm{im},i} - C_{\mathrm{im},i-1}}{\frac{z_i - z_{i-2}}{2}} = -k_{\mathrm{ex}}^{i}(C_{\mathrm{im},i} - C_{\mathrm{im},i-1}) \quad \text{for } 2 \le i \le n \tag{29}$$

hence,

$$k_{\mathrm{ex}}^{1} = \frac{a(0)\,D_0}{\frac{z_1}{2}} \quad \text{for zone } i = 1 \tag{30}$$

$$k_{\mathrm{ex}}^{i} = \frac{a(z_{i-1})\,D_0}{\frac{z_i - z_{i-2}}{2}} \quad \text{for the zones } i = 2\ldots n \tag{31}$$

which means that the mass transfer coefficient, k_{ex}^{i}, between the zones $i-1$ and i depends on, $a(z)$, the total cross-sectional area of the immobile regions per unit volume of the soil column. The mass transfer equation in the immobile region can thus be discretised as follows:

$$\begin{aligned}
\frac{\mathrm{d}C_{\mathrm{im},1}^{\mathrm{tot}}}{\mathrm{d}t} &= \frac{k_{\mathrm{ex}}^{1}}{\theta_{\mathrm{im},1}}(C_{\mathrm{mob}} - C_{\mathrm{im},1}) - \frac{k_{\mathrm{ex}}^{2}}{\theta_{\mathrm{im},1}}(C_{\mathrm{im},1} - C_{\mathrm{im},2}) \\
\frac{\mathrm{d}C_{\mathrm{im},i}^{\mathrm{tot}}}{\mathrm{d}t} &= \frac{k_{\mathrm{ex}}^{i}}{\theta_{\mathrm{im},i}}(C_{\mathrm{im},i-1} - C_{\mathrm{im},i}) - \frac{k_{\mathrm{ex}}^{i+1}}{\theta_{\mathrm{im},i}}(C_{\mathrm{im},i} - C_{\mathrm{im},i+1}),\ i = 2\ldots n-1 \\
\frac{\mathrm{d}C_{\mathrm{im},i}^{\mathrm{tot}}}{\mathrm{d}t} &= \frac{k_{\mathrm{ex}}^{n}}{\theta_{\mathrm{im},n}}(C_{\mathrm{im},n-1} - C_{\mathrm{im},n}).
\end{aligned} \tag{32}$$

The BTCs of DNB in our system were modeled using the respective values of the hydrodynamic and column parameters determined in independent experiments (see Section 3.1). Calculations including and neglecting hydrodynamic dispersion as determined from experiments with the conservative tracer (Section 3.1) were not significantly different. Thus, the modeling of DNB BTCs was performed neglecting dispersive processes if not otherwise stated.

Both, the fraction and the maximal length of the immobile region, f_{im} and d, turned out to be interdependent and, thus, poorly identifiable. Generally, shorter pore lengths resulted in smaller fractions of immobile regions. The reason for this identifiability problem is that smaller cross-sectional areas of the pores result in increased retardation of the diffusion process, what leads to shorter penetration depths. For our system the maximal length of the pores of the immobile regions, d, was set to be 100 μm. This estimate is based on examinations of REM images of the clay aggregates (Fig. 2) assuming a typical aggregate size of about 20 μm and a tortuosity of about five. This led to fractions of the immobile region, f_{im}, that were smaller than 0.2% (Table 8), which was in accordance to the findings of the experiments with the conservative tracer (Section 3.1).

The geometry and the distribution of sorption sites within the immobile regions of sandmont are not known. However, testing different assumptions on the functional dependencies of $a(z)$ and $s_{max,\,im}(z)$ allowed an approximate evaluation of the geometry and site distribution of the immobile region within the porous medium. Table 8 summarises the different combinations of hypotheses tested with the respective parameter and χ^2 values. The cross-sectional area of the immobile regions, $a(z)$, was assumed to be either constant (lines 1, 2) or to increase exponentially with depth (lines 3–5). Regarding the sorption site distribution, a constant distribution (lines 1, 2) as well as a linear (line 4) or quadratic (lines 2, 5) increase of sites with depth were considered. In addition, a radial geometry of the immobile region with an according decrease of sorption sites with depth was examined (line 6). The parameter values given in Table 8 were fitted simultaneously to the data of all five continuous flow column experiments

Table 8
Fitted parameter and χ^2 values calculated for the BTCs of DNB by the two-region model considering retarded intra-particle diffusion. One set of parameter values described the whole set of BTCs measured (see text). Models of increasing complexity with respect to geometry and distribution of sorption sites are compared

$a(z)=[\mathrm{cm}^{-1}]$	$s_{max,\,im\,(z)}=$ [μmol kg^{-1} cm^{-2}]	γ [−]	κ [a] [cm^{-1}], [b][cm^{-2}]	$S_{max,\,im}$ [μmol kg^{-1}]	$S_{max,\,mob}$ [μmol kg^{-1}]	f_{im} [−]	χ^2
Const	const	−	−	230	299	$7.2\cdot10^{-5}$	1580
Const	[b]const$\cdot(\kappa z^2+1)$	−	500	207	294	$1.1\cdot10^{-4}$	1409
Const$\cdot e^{-\gamma z}$	const	321	−	232	294	$6.2\cdot10^{-5}$	1341
Const$\cdot e^{-\gamma z}$	[a]const$\cdot(\kappa z+1)$	447	84	233	286	$1.0\cdot10^{-4}$	1239
Const$\cdot e^{-\gamma z}$	[b]const$\cdot(\kappa z^2+1)$	727	1122	265	250	$1.6\cdot10^{-3}$	872
$(d-z)^2$	$(d-z)^2$	−	−	201	300	$1.5\cdot10^{-5}$	1645

The units and values of the constants, const, result from Eqs. (18) and (19). γ and κ are auxiliary parameters. The units of κ change according to the function chosen describing $s_{max,\,im}$ ([a, b]).

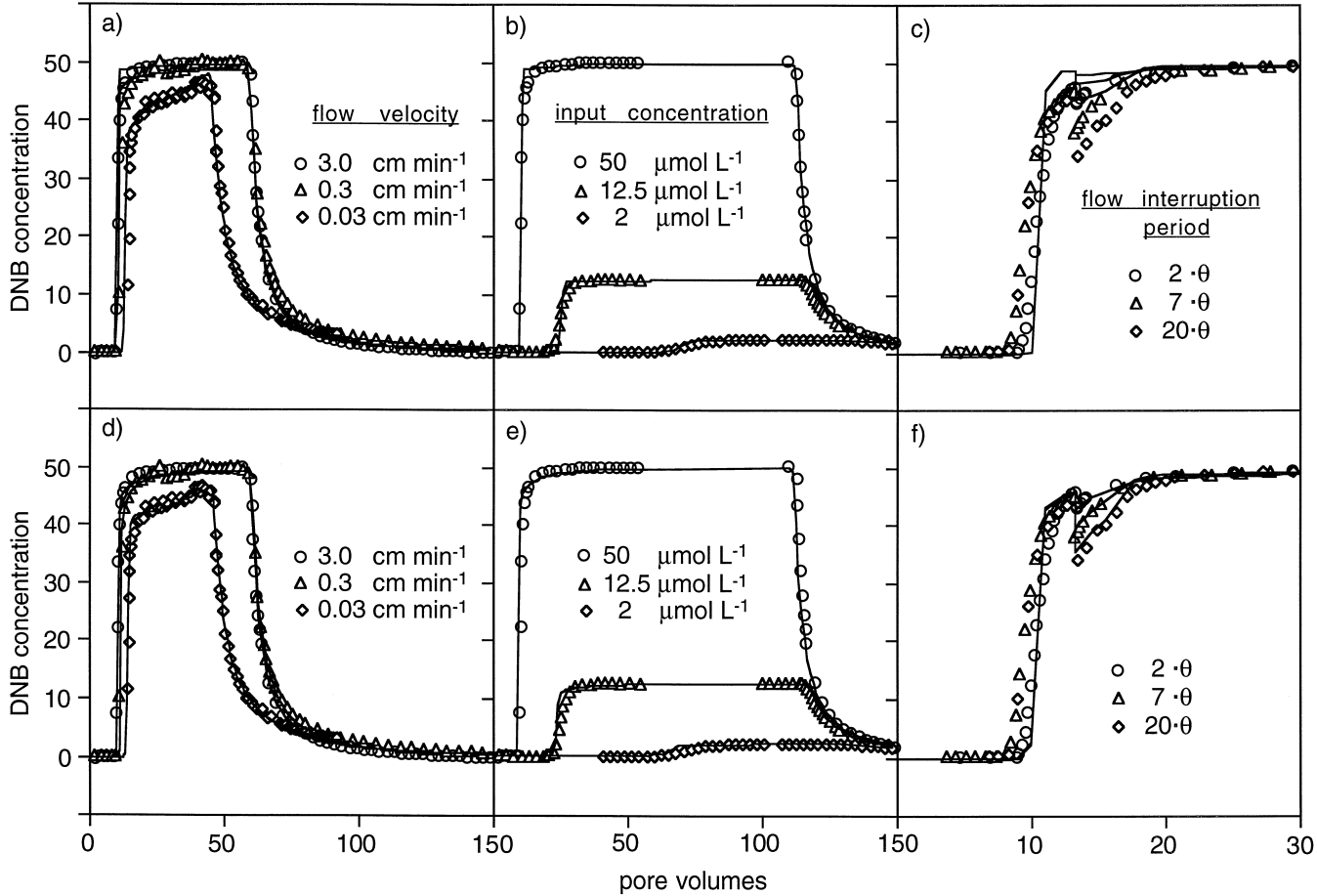

Fig. 8. BTCs of DNB in a column containing clay coated sand matrix. Markers represent measured data, lines show results of calculations with the two-region model that considers nonlinear sorption and retarded solute diffusion within the clay aggregates (see Section 3.3.2 and Table 8 for parameter values). In contrast to the classical two-region model (see Section 3.3.1; Fig. 6) a single set of parameter values was sufficient to describe the entire set of miscible displacement experiments conducted. (a–c) Three parameter model. (d–e) Five parameter model (see text). Note the different scales of the abscissa.

(conducted at different flow velocities and DNB input concentrations; see Table 3). The data of the three interrupted flow experiments were simulated with the resulting sets of parameter values. The simplest model (constant geometry and site distribution; line 1 in Table 8) with only three adjustable parameters ($S_{max,\,mob}$, $S_{max,\,im}$, and f_{im}) described the data reasonably well (Fig. 8a–c). The decreasing χ^2 values given in Table 8 indicate that more complex functions with respect to geometry and site distribution of the aggregates described the data somewhat better. Note that the spherical model led to the highest χ^2 value due to the inherent decrease of sorption sites within homogeneous spheres. A spherical geometry but an increasing amount of sorption sites with z yielded lower χ^2 values (not shown). The best fit was obtained when the pore cross-sectional area decreased exponentially with z and the sorption site density increased quadratically with the pore depth (Fig. 8d–f). The relatively small differences in χ^2 between some of the models indicate that the exact form of these two functions was poorly identifiable. However, the results indicate that the pore cross-sectional area of the aggregates in sandmont decreased with pore depth whereas the sorption site density increased. This may be the case if the pore volume increasingly branches towards the centre of the aggregates giving rise to an increasing ratio of clay surface sites to pore water volume despite a decrease in the total pore cross-sectional area. Although such a situation is conceivable considering the complex structure of clay-organic aggregates (Fig. 2), we do not have independent experimental data to prove this hypothesis.

Earlier work suggests that strongly sorbing solutes may be subject to enhanced effective dispersivity (e.g., van Genuchten et al., 1977; Sugita and Gillham, 1995b). In our systems, an increase of the parameter values of λ up to 100-fold over the respective dispersivity values obtained with the conservative tracer only slightly improved χ^2 (not shown). The extent of additional dispersion increased with decreasing DNB input concentrations, consistent with stronger sorption at lower concentrations and, hence, with a more distinct pore scale variation in the retardation factor as it was proposed by Sugita and Gillham (1995a). However, the effect of dispersion was negligible compared to the effects of nonlinear sorption and retarded intra-particle diffusion.

The tailing at the top of the concentration front and the changes in aqueous solute concentration during flow interruption were effects caused by nonequilibrium mass transfer. The tailing of the desorption front, however, was mainly caused by the

Table 9
Parameter values fitted with different values of α and K_{LF} to determine the sensitivity of the model to the isotherm parameters used. The simplest model assuming constant geometry and site distribution was chosen because in this case only three parameters were fitted. Measured isotherm parameters obtained in independent sorption experiments led to best results

α [−]	K_{LF} [l$^{\alpha}$ μmol$^{-\alpha}$]	$S_{max,\,mob}$ [μmol kg^{-1}]	$S_{max,\,im}$ [μmol kg^{-1}]	f_{im} [−]	χ^2
0.57[a]	0.12[a]	301	215	$6.8\cdot10^{-5}$	1584
0.57	0.10	260	329	$7.5\cdot10^{-5}$	1942
0.57	0.14	284	163	$4.6\cdot10^{-5}$	2392
0.47	0.12	304	201	$6.9\cdot10^{-5}$	23312
0.67	0.12	269	100	$3.3\cdot10^{-5}$	3442

[a] Isotherm parameters obtained experimentally.

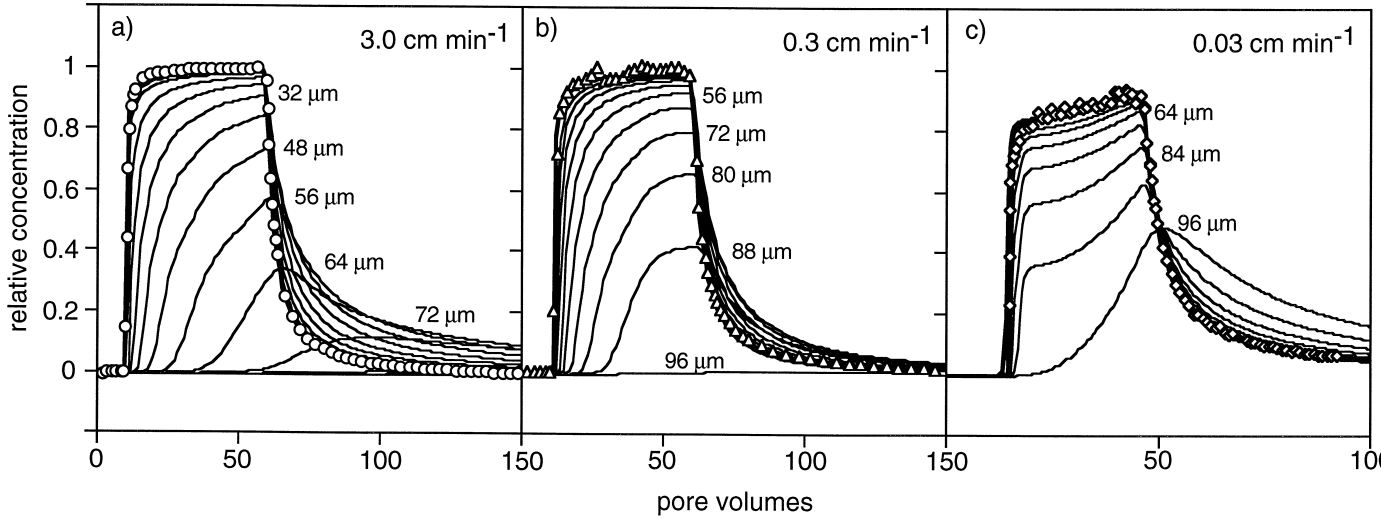

Fig. 9. Effect of pore water velocity on DNB concentrations in the mobile region at the column outlet (thick line) and at different penetration depths within the pores of the immobile regions (thin lines). Dots represent measured data at the column outlet ($C_0 = 50\ \mu\text{mol l}^{-1}$). Note the different scales of the abscissa.

nonlinearity of the sorption isotherm. In order to determine the sensitivity of the estimated parameter values with respect to the isotherm parameters used, parameter estimations with different values of α and K_{LF} were performed (Table 9). Small changes in the isotherm parameters significantly decreased the quality of the fit. This confirms that the shape of the BTCs was strongly determined by the shape of the DNB isotherms and supports the correctness of the isotherm parameter values as determined by the in situ incremental column method as described in Section 3.2.2.

Fig. 9 shows the transients of the DNB concentrations at the end of the column in the mobile region and at different depths within the aggregates for the three different flow velocities. The penetration depth of the solutes increased with decreasing flow velocity and the DNB concentration was not distributed homogeneously within the immobile region. Obviously, such effects could not be described by the model discussed in Section 3.3.1., which considered immobile regions but no concentration gradients.

4. Summary and conclusions

In this work, we have examined the effects of nonlinear sorption, nonequilibrium mass transfer and uneven distribution of reactive surfaces on solute transport in porous media. The experimental investigation of these phenomena was possible using a mixture of inert quartz sand and reactive clay aggregates. This porous medium contained a very small fraction of immobile regions, which hosted a significant fraction of the reactive clay surfaces present. Using a multiple tracer approach, different physical and chemical processes (hydrodynamic transport, intra-aggregate diffusion, linear and nonlinear sorption) were identified and quantified. Various sets of batch adsorption and miscible displacement experiments were performed covering a wide range of time scales and other experimental conditions. In miscible displacement experiments, the nonlinear sorption of the reactive tracer was reflected in sharp adsorption and tailing desorption fronts of the BTCs. The effect of nonequilibrium mass transfer was most evident from the tailing of the self-sharpened adsorption fronts of these BTCs and from the distinct changes in solute concentration during flow interruption.

The experimental data of the nonlinearly sorbing solute were modeled with the data analysis program AQUASIM. Calculations showed that both nonlinear sorption and nonequilibrium mass transfer had a strong impact on solute transport. A two-region model with completely mixed immobile regions considering chemical equilibrium and nonlinear sorption was able to describe the results of individual miscible displacement experiments. However, with this model different sets of parameter values were necessary to describe experiments conducted at different flow rates. This indicated that the relevant time scales of the mass transfer processes depended on the flow rate. To account for such processes diffusion within the immobile region was described explicitly in a two-region model considering nonlinear sorption and retarded intra-aggregate diffusion. This model successfully described the results of the *entire* set of miscible displacement experiments using a *single* set of parameter values. In contrast to other diffusion models, any distribution of sorption sites within the immobile regions can be considered in this approach. In our systems, the concentration of reactive sites turned out

to increase with the depth of the aggregates. Since the hydrodynamic and most of the sorption isotherm parameters were known from independent experiments, at most, three to five parameter values were fitted simultaneously with the aid of data from five column experiments at three different pore water velocities and with three different input concentrations.

Our study demonstrates that complex coupled processes such as nonlinear sorption and nonequilibrium mass transfer can be identified from appropriate experimental data. However, a set of complementary experiments performed under very different conditions in combination with an advanced data analysis tool was necessary to derive unambiguous results. It was shown that, in contrast to the nonreactive solutes, the transport of sorbing solutes may strongly be affected by diffusive exchange with a very small volume fraction of immobile regions, if a significant fraction of sorption sites is located within such aggregates. The comparison of batch and column sorption isotherms revealed that the number of sorption sites determined by batch techniques significantly overestimated the conditions within the columns. This was attributed to a disaggregation of clay clusters in batch experiments during stirring, which resulted in exposure of additional surfaces.

Our study was performed in model systems designed to mimic processes occurring in natural porous media. Since reactive solid surfaces in soils and aquifers often are present in aggregates, our results are generally applicable to the transport and transformation of pollutants that strongly interact with poorly accessible surfaces. Our results suggest that slow (de)sorption and limited degradability, as often observed in the field (e.g., the works of Steinberg et al., 1987; Miller and Pedit, 1992; Hatzinger and Alexander, 1995; Nielsen et al., 1995), may be due to grain scale retarded intra-aggregate diffusion processes.

However, further work in flow-through systems is needed to evaluate the effects of additional processes that are known to affect the sorption and reactivity of contaminants. In the case of nitroaromatic compounds (NACs), competitive adsorption in mixtures of NACs and cation exchange at clay minerals play an important role. Such investigations are currently in progress in our laboratory. The applicability of the conceptual model presented has also been evaluated under unsaturated flow conditions and will be presented elsewhere (Fesch et al., 1998).

5. Notation

A	cross-sectional area of model column [cm^2]
$a(z)$	surface area of pores building the immobile region per unit column volume [cm^{-1}]
C	solution-phase solute concentration [μmol l^{-1}]
C_{mob}, C_{im}	solution-phase solute concentration in mobile, immobile region [μmol l^{-1}]
C_{mob}^{tot}, C_{im}^{tot}	total solute concentration in mobile, immobile region [μmol l^{-1}]

C_n, C_{n+1}	constant solution-phase solute concentrations at column inlet for incremental sorption isotherm determination [μmol l^{-1}]
$C_{meas,i}$	measured solution-phase solute concentration at column outlet at time t_i [μmol l^{-1}]
$C_{calc,i}$	calculated solution-phase solute concentration at column outlet at time t_i [μmol l^{-1}]
$C(t)$	solution-phase solute concentration at time t [μmol l^{-1}]
D	hydrodynamic dispersion coefficient [cm^2 min^{-1}]
D_0	molecular diffusion coefficient in water [cm^2 min^{-1}]
d	maximal length of the pores of the immobile regions [cm]
f_{im}	fraction of the immobile region [−]
F_{im}	solute flux in immobile region of aggregates [mol cm^{-3} min^{-1}]
f_{oc}	fraction of particulate organic carbon $\left[\frac{g_{oc}}{g_{sorbent}}\right]$
K_{LF}	Langmuir–Freundlich partition coefficient (an affinity (adsorption energy) parameter) [l^{α} μmol$^{-\alpha}$]
k_{ex}	exchange coefficient between regions [min^{-1}]
L	column length [cm]
R	retardation factor [−]
S	sorbed-phase solute concentration [μmol kg^{-1}]
S_{mob}, S_{im}	sorbed-phase solute concentration in mobile, immobile region [μmol kg^{-1}]
$S_{im}(z)$	sorbed-phase solute concentration per unit pore depth z of the immobile region [μmol kg^{-1} cm^{-1}]
S_{max}	maximum sorbed-phase solute concentration [μmol kg^{-1}]
$S_{max,\,mob}$, $S_{max,\,im}$	maximum sorbed-phase solute concentration in mobile region [μmol kg^{-1}]
$s_{max,\,im}(z)$	maximum sorbed-phase solute concentration per unit pore depth z of the immobile region [μmol kg^{-1} cm^{-1}]
t	time [min]
$t_{n,n+1}$	time when column inlet concentration was switched from C_n to C_{n+1} [min]
t_0	hydraulic retention time [min]; $t_0 = \frac{L}{v}$;
v	pore water velocity [cm min^{-1}]
x	distance along the column [cm]
z	spatial coordinate along the pores of the immobile region [cm]
α	Langmuir–Freundlich isotherm exponent (power function) [−] $0 < \alpha \leq 1$
γ	fitting parameter [−]
κ_a, κ_b	fitting parameter [cm^{-1}], [cm^{-2}] (see Table 8)
ρ_s	sorbent density [kg l^{-1}]
ρ_b	bulk density [kg l^{-1}]; $\rho_b = \rho_s(1-\theta)$
Γ	smoothed value of the slope of the measured BTC [−]
σ_{conc}	standard deviation of solute concentrations [μmol l^{-1}]

σ_{meas}	standard deviation of solute concentrations including uncertainties in time measurements [μmol l^{-1}]
σ_{time}	standard deviation of time measurements [min]
ϕ	porosity [l l^{-1}]
ϕ_{mob}, ϕ_{im}	porosity of mobile, immobile region [l l^{-1}]
θ	volumetric water content [l l^{-1}]
θ_{mob}, θ_{im}	volumetric water content of mobile, immobile region [l l^{-1}]

Acknowledgements

We thank Emil Franov for conducting preliminary column experiments. C_{org} was measured by Antonin Mares, BET measurements were carried out by Daniel Kobler. We are indebted to Thomas Gimmi, Rick Devlin, William Ball, and Peter Grathwohl who carefully reviewed the manuscript, and to Sabine Koch, Peter Lehmann, and Hauke Harms who made valuable comments. Financial support was provided by the Board of the Swiss Federal Institutes of Technology (OPUS-project), the Swiss National Science Foundation (grant No. 8220-04617), and by the priority research program 1993–1997 of EAWAG.

References

Aris, R., Amundson, N.R., 1973. Mathematical Methods in Engineering: 2. First-Order Partial Differential Equations with Applications. Prentice-Hall, Englewood Cliffs, NJ.

Bajracharya, K., Barry, D.A., 1997. Nonequilibrium solute transport parameters and their physical significance: numerical and experimental results. J. Cont. Hydrol. 24, 185–204.

Berglund, S., Cvetkovic, V., 1996. Contaminant displacement in aquifers: coupled effects of flow heterogeneity and nonlinear sorption. Water Resour. Res. 32 (1), 23–32.

Bosma, W.J.P., van der Zee, S.E.A.T.M., 1995. Dispersion of a continuously injected, nonlinearly adsorbing solute in chemically or physically heterogeneous porous formations. J. Contam. Hydrol. 18, 181–198.

Brusseau, M.L., 1994. Transport of reactive contaminants in heterogeneous porous media. Rev. Geophys. 32 (3), 285–313.

Brusseau, M.L., Rao, P.S.C., 1989. Sorption nonideality during organic contaminant transport in porous media. CRC Crit. Rev. Environ. Contam. 19, 33–99.

Brusseau, M.L., Rao, P.S.C., Jessup, R.E., Davidson, J.M., 1989. Flow interruption: a method for investigating sorption equilibrium. J. Contam. Hydrol. 4, 223–240.

Brusseau, M.L., Hu, Q., Srivastava, R., 1997. Using flow interruption to identify factors causing nonideal contaminant transport. J. Contam. Hydrol. 24, 205–219.

Bürgisser, C.S., Cernik, M., Borkovec, M., Sticher, H., 1993. Determination of nonlinear adsorption isotherms from column experiments: an alternative to batch studies. Environ. Sci. Technol. 27, 943–948.

Cameron, D.R., Klute, A., 1977. Convective-dispersive solute transport with a combined equilibrium and kinetic adsorption model. Water Resour. Res. 13 (1), 183–188.

Coats, K., Smith, B., 1964. Dead end pore volume and dispersion in porous media. Soc. Petr. Eng. 4 (3), 73–84.

Fesch, C., Lehmann, P., Haderlein, S.B., Hinz, C., Schwarzenbach, R.P., Flühler, H., 1998. Effect of water content on solute transport in aggregated porous media. J. Contam. Hydrol., in press.

Fujita, T., 1983. Substituent effects in the partition coefficients of disubstituted benzenes: bi-directional Hammett-type relationships. In: Taft, R.W. (Ed.), Progress in Physical Organic Chemistry, Vol. 14, Wiley, New York, pp. 75–113.

Glueckauf, E., Coates, J.I., 1947. Theory of chromatography: IV. The influence of incomplete equilibrium on the front boundary of chromatographs and on the effectiveness of separations. J. Chem. Soc., Part II, pp. 1315–1321.

Haderlein, S.B., Schwarzenbach, R.P., 1993. Adsorption of substituted nitrobenzenes and nitrophenols to mineral surfaces. Environ. Sci. Technol. 27, 316–326.

Haderlein, S.B., Weissmahr, K.W., Schwarzenbach, R.P., 1996. Specific adsorption of nitroaromatic explosives and pesticides to clay minerals. Environ. Sci. Technol. 30 (2), 612–622.

Haggerty, R., Gorelick, S.M., 1995. Multiple-rate mass transfer for modeling diffusion and surface reactions in media with pore-scale heterogeneity. Water Resour. Res. 31 (10), 2383–2400.

Hansch, C., Leo, A., 1979. Substituent Constants for Correlation Analysis in Chemistry and Biology. Wiley, New York.

Harms, H., Zehnder, A.J.B., 1995. Bioavailability of sorbed 3-chlorodibenzofuran. Appl. Environ. Microbiol. 61 (1), 27–33.

Hatzinger, P.B., Alexander, M., 1995. Effect of aging of chemicals in soil on their biodegrability and extractibility. Environ. Sci. Technol. 29 (2), 537–545.

Helfferich, F.G., Carr, P.W., 1993. Non-linear waves in chromatography: I. Waves, shocks and shapes. J. Chromatogr. 629, 97–122.

Hu, Q., Brusseau, M.L., 1996. Transport of rate-limited sorbing solutes in an aggregated porous medium: a multiprocess non-ideality approach. J. Contam. Hydrol. 24, 53–73.

Jury, W.A., Flühler, H., 1992. Transport of chemicals through soil: mechanisms, models, and field applications. Adv. Agron. 47, 141–201.

Kinniburgh, D.G., 1986. General purpose adsorption isotherms. Environ. Sci. Technol. 20, 895–904.

Klausen, J., Tröber, S.P., Haderlein, S.B., Schwarzenbach, R.P., 1995. Reduction of substituted nitrobenzenes by Fe(II) in aqueous mineral suspensions. Environ. Sci. Technol. 29 (9), 2396–2404.

Koch, S., Fluehler, H., 1993. Non-reactive solute transport with micropore diffusion in aggregated porous media determined by a flow-interruption method. J. Contam. Hydrol. 14, 39–54.

Kreyszig, E., 1979. Statistische Methoden und ihre Anwendung. Vandenhoek and Rupprecht, Göttingen.

Lapidus, L., Amundson, N.R., 1952. Mathematics of adsorption beds: VI. The effect of longitudinal diffusion in ion exchange and chromatographic columns. J. Phys. Chem. 56, 984–988.

Leo, A., Hansch, C., Elkins, D., 1971. Partition coefficients and their uses. Chem. Rev. 71, 702–709.

LeVeque, R.J., 1990. Numerical Solution of Conservative Laws. Birkhäuser, Basel.

Martell, A.E., Smith, R.M., 1982. Critical Stability Constants. Plenum, New York.

McBride, J.F., Brockman, F.J., Szecsody, J.E., Streile, G.P., 1992. Kinetics of quinoline biodegradation, sorption and desorption in a clay-coated model soil containing a quinoline-degrading bacterium. J. Contam. Hydrol. 9, 133–154.

Miller, M.E., Alexander, M., 1991. Kinetics of bacterial degradation of benzylamine in a montmorillonite suspension. Environ. Sci. Technol. 25 (2), 240–245.

Miller, C.T., Pedit, J.A., 1992. Use of reactive surface-diffusion model to describe apparent sorption-desorption hysteresis and abiotic degradation of lindane in a subsurface material. Environ. Sci. Technol. 26 (7), 1417–1427.

Murali, V., Aylmore, L.A.G., 1980. No-flow equilibration and adsorption dynamics during ionic transport in soils. Nature 283, 467–469.

Nakamura, Y., Yamagishi, A., Iwamoto, T., Koga, M., 1988. Adsorption properties of montmorillonite and synthetic saponite as packing materials in liquid-column chromatography. Clays Clay Minerals 36 (6), 530–536.

Nelder, J.A., Mead, R., 1965. A simplex method for function minimization. Comput. J. 7, 308–313.

Nielsen, P.H., Bjarnadóttir, H., Winter, P.L., Christensen, T.H., 1995. In situ and laboratory studies on the fate of the specific organic compounds in an anaerobic landfill leachate plume, 2. Fate of aromatic and chlorinated aliphatic compounds. J. Contam. Hydrol. 20, 51–56.

Ogram, A.V., Jessup, R.E., Ou, L.T., Rao, P.S.C., 1985. Effects of sorption on biological degradation rates of (2,4-dichlorophenoxy) acetic acid in soils. Appl. Environ. Microbiol. 49 (3), 582–587.

Parker, J.C., van Genuchten, M.T., 1984. Determining transport parameters from laboratory and field tracer experiments, Blacksburg, VA.

Petzold, L., 1983. A description of DASSL: a differential/algebraic system solver. In: Stepleman, R. (Ed.), Scientific Computing, IMACS/North-Holland, Amsterdam, pp. 65–68.

Pignatello, J.J., Xing, B.S., 1996. Mechanisms of slow sorption of organic chemicals to natural particles. Environ. Sci. Technol. 30 (1), 1–11.

Ralston, M.L., Jennrich, R.I., 1978. Dud, a derivate-free algorithm for nonlinear least squares. Technometrics 20 (1), 7–14.

Rao, P.S.C., Rolston, D.E., Jessup, R.E., Davidson, J.M., 1980. Solute transport in aggregated porous media: theoretical and experimental evaluation. Soil Sci. Soc. Am. J. 44, 1139–1146.

Reichert, P., 1994. AQUASIM—a tool for simulation and data analysis of aquatic systems. Wat. Sci. Technol. 30 (2), 21–30.

Reichert, P., 1995. Design techniques of a computer program for the identification of processes and simulation of water quality in aquatic systems. Environ. Software 10 (3), 199–210.

Sachs, L., 1982. Applied Statistics: A Handbook of Technics. Springer, New York.

Sardin, M., Schweich, D., 1991. Modeling the nonequilibrium transport of linearly interacting solutes in porous media: a review. Water Resour. Res. 27, 2287–2307.

Schweich, D., Sardin, M., 1981. Adsorption, partition, ion exchange and chemical reaction in batch reactors or in columns—a review. J. Hydrol. 50, 1–33.

Selim, H.M., Davidson, J.M., Mansell, R.S., 1976. Evaluation of a two-site adsorption–desorption model for describing solute transport in soil, Proceedings of the Computer Simulation Conference, Am. Inst. of Chem. Eng., Washington, DC, pp. 444–448.

Serjeant, E.P., Dempsey, B., 1979. Ionisation Constants of Organic Acids in Aqueous Solution. Pergamon, Oxford.

Sigg, L., 1987. Surface chemical aspects of the distribution and fate of metal ions in lakes. In: Stumm, W. (Ed.), Aquatic Surface Chemistry, Wiley-Interscience, New York.

Simon, W., Reichert, P., 1997. An extension of AQUASIM to saturated soil columns. Ground Water, submitted.

Sposito, G., 1990. Molecular models of ion adsorption on mineral surfaces. In: Hochella, M.F., Jr., White, A.F. (Eds.), Mineral–Water Interface Geochemistry, Washington DC, pp. 261–279.

Spurlock, F.C., Huang, K., van Genuchten, M.T., 1995. Isotherm nonlinearity and nonequilibrium sorption effects on transport of fenuron and monuron in soil columns. Environ. Sci. Technol. 29 (4), 1000–1007.

Steinberg, S.M., Pignatello, J.J., Sawhney, B.L., 1987. Persisitence of 1,2-dibromoethane in soils: Entrapment in intraparticle micropores. Environ. Sci. Technol. 21 (12), 1201–1208.

Stone, A.T., Torrents, A., Smolen, J., Vasudevan, D., Hadley, J., 1993. Adsorption of organic compounds possessing ligand donor groups at the oxide/water interface. Environ. Sci. Technol. 27 (5), 895–909.

Sugita, F., Gillham, R.W., 1995a. Pore scale variation in retardation factor as a cause of nonideal reactive breakthrough curves: 1. Conceptual model and its evaluation. Water Resour. Res. 31 (1), 103–112.

Sugita, F., Gillham, R.W., 1995b. Pore scale variation in retardation factor as a cause of nonideal reactive breakthrough curves: 3. Column investigations. Water Resour. Res. 31 (1), 121–128.

Sugita, F., Gillham, R.W., Mase, C., 1995. Pore scale variation in retardation factor as a cause of nonideal reactive breakthrough curves: 2. Pore network analysis. Water Resour. Res. 31 (1), 113–119.

Talibudeen, O., 1981. Cation exchange on soils. In: Greenland, D.J., Hayes, M.H.B. (Eds.), The Chemistry of Soil Processes, Wiley, Chichester, pp. 115–178.

Toride, N., Leij, F.J., van Genuchten, M.T., 1995. The CXTFIT Code for Estimating Transport Parameters from Laboratory or Field Tracer Experiments, Version 2.0., US Department of Agriculture, Riverside, CA, USA.

Torrents, A., Stone, A.T., 1991. Hydrolysis of phenyl picolinate at the mineral/water interface. Environ. Sci. Technol. 25, 143–149.

Unger, K.K.E., 1989. Handbuch der HPLC. Git Verlag, Darmstadt.

van der Zee, S.E.A.T.M., van Riemsdijk, W.H., 1986. Sorption kinetics and transport of phosphate in sandy soil. Geoderma 38, 293–309.

van Genuchten, M.T., Wierenga, P.J., 1976a. Mass transfer studies in sorbing porous media: 1. Analytical solutions. Soil Sci. Soc. Am. J. 40, 473–480.

van Genuchten, M.T., Wierenga, P.J., 1976b. Numerical solution for convective dispersion with intra-aggregate diffusion and non-linear adsorption. In: Vansteenkiste, G.C. (Ed.), System Simulation in Water Resources, North-Holland, Amsterdam, pp. 275–292.

van Genuchten, M.T., Wierenga, P.J., O'Connor, G.A., 1977. Mass transfer studies in sorbing porous media: III. Experimental evaluation with 2,4,5-T. Soil Sci. Soc. Am. J. 41, 278–285.

van Leer, B., 1974. Towards the ultimate conservative difference scheme: II. Monotonicity and conservation combined in a second order scheme. J. Comput. Phys. 14, 361–370.

Voudrias, E.A., Reinhard, M., 1986. Abiotic Organic Reactions at Mineral Surfaces. In: Davis, J.A., Hayes, K.F. (Eds.), Geochemical Processes at Mineral Surfaces, Vol. 323, Chap. 22, American Chemical Society, Washington, DC, pp. 462–468.

Weber, W.J.J., McGinley, P.M., Katz, L.E., 1991. Sorption phenomena in surface systems: concepts, models and effects on contaminant fate and transport. Water Res. 25 (5), 499–528.

Weissmahr, K.W., Haderlein, S.B., Schwarzenbach, R.P., 1998. Complex formation of soil minerals with nitroaromatic explosives and other π-acceptors. Soil Sci. Soc. Am. J. 62 (2), in press.

Wu, S., Gschwend, P.M., 1986. Sorption kinetics of hydrophobic organic compounds to natural sediments and soils. Environ Sci. Technol. 20, 717–725.

Xu, L., Brusseau, M.L., 1996. Semianalytical solution for solute transport in porous media with multiple spatially variable reaction processes. Water Resour. Res. 32 (7), 1985–1991.

Yiacoumi, S., Rao, A.V., 1996. Organic solute uptake from aqueous solutions by soil: a new diffusion model. Water Resour. Res. 32 (2), 431–440.

Young, D.F., Ball, W.P., 1994. A priori simulation of tetrachloroethene transport through aquifer material using an intraparticle diffusion model. Environ. Prog. 13 (1), 9–20.

Young, D.F., Ball, W.P., 1995. Effects of column conditions on the first-order rate modeling of nonequilibrium solute breakthrough. Water Resour. Res. 31 (9), 2181–2192.

Zachara, J.M., Ainsworth, C.C., Smith, S.C., 1990. The sorption of *N*-heterocyclic compounds on reference and subsurface smectite clay isolates. J. Contam. Hydrol. 6, 281–305.